MATERIALS AND METHODS

1. ZEBRAFISH (*Danio rerio*) LINES

The transgenic *sod1* zebrafish lines used in this work were provided by Dr. Christine E. Beattie, Center for Molecular Neurobiology and Department of Neuroscience, The Ohio State University, Columbus OH 43210, USA.

She provided us two stable transgenic zebrafish lines: WT os4 (we will hereafter refer to these animals as wtSod1) and G93R os10 (we will hereafter refer to these fish as mSod1). Because zebrafish live at a lower temperature (28°C) than mammals (37°C), the zebrafish *sod1* gene and regulatory regions were used to generate the transgenic animals, in order to avoid any effect of temperature on the enzyme functionality. Both transgenic zebrafish lines were generated injecting, into one-cell stage embryos, a DNA construct composed of a 21-kb zebrafish genomic region containing the endogenous *sod1* gene (5.06 kb) and *sod1* promoter and flanking sequences (11.7 kb upstream and 4.5 kb downstream) followed by the zebrafish *heat shock protein 70* (*hsp70*) promoter driving the expression of the fluorescent protein DsRed, for the identification of the transgenic embryos. The embryos were obtained intercrossing adult wild-type hybrids of *AB and Tupfel long fin strains. While the wtSod1 line contains ~42 copies of the wild-type form of the *sod1* gene, the mSod1 line integrated a higher number (~165 copies) of mutated *sod1* gene (348 G>C; NCBI Reference Sequence NP_571369.1), overexpressing a mutated form of the *Sod1* protein where the glycine 93 is changed to arginine (G93R) (Ramesh et al., 2010), a mutation affecting an evolutionarily conserved amino acid that is often mutated in FALS (Elshafey et al., 1994; Orrell et al., 1999). Both lines are characterized by an ubiquitous overexpression of Sod1, consistent with the expression profile of the endogenous *sod1* gene and, in particular, by a threefold increase in the steady-state Sod1 protein levels in the brain and a fourfold increase in the spinal cord, at one year of age, compared with non-transgenic siblings (Ramesh et al., 2010). To maintain the mutant transgenic lines, wtSod1 and mSod1 zebrafish were outcrossed, in group mating, to the AB and TL wild-type lines present in our facility to increase the variability of the genetic background. Since we were interested in the phenotype associated to the moderate over-expression of wild-type and mutant *sod1*, we used adult heterozygous transgenic fish. In experiments performed in embryos and larvae, we studied the transgenic progeny generated intercrossing wtSod1 or mSod1 heterozygous adult zebrafish. We identified transgenic embryos overexpressing wtSod1 or mSod1 (~75 %) thanks to the expression of the fluorescent protein DsRed while the non-transgenic progeny (~25 %) was used as control (we will hereafter refer to these animals as Ctrl).

2. FISH MAINTENANCE

Zebrafish were maintained in 28°C, pH 7.4 and 500 µS conductivity water on a 14 hours light/10 hours dark cycle with the ZebTEC Stand-Alone "Active Blue" Technology system (Tecniplast S.p.A., 21020 Buguggiate (VA) Italy) and bread according to established procedures (Westerfield, 2000).

Embryos were collected by natural spawning and raised at 28°C in embryo water (0.1% Instant Ocean® Synthetic Sea Salt (Tecniplast S.p.A., 21020 Buguggiate (VA) Italy), 1.2 mM $NaHCO_3$ (S5761, Sigma-Aldrich®, St. Louis, MO, USA), 1.1 mM $CaSO_4$ (C3771, Sigma-Aldrich®, St. Louis, MO, USA), 0.1% methylene blue (M9140, Sigma-Aldrich®, St. Louis, MO, USA) in petri dishes. Embryos, used in whole-mount immunofluorescence experiments, were raised in 0.003% 1-phenyl-2 thiourea (PTU, P7629, Sigma-Aldrich®, St. Louis, MO, USA), from 1-day post fertilization (dpf) to avoid pigmentation. Staging of embryos was done according to Kimmel et al. (Kimmel et al., 1995).

3. EXTERNALLY VISIBLE ANATOMY AND BODY WEIGHT EVALUATION

To asses if the overexpression of wtSod1 or mSod1 affects adult zebrafish anatomy, twelve months old heterozygous wtSod1 and mSod1 zebrafish and AB zebrafish (Ctrl) were weighted, photographed with the rear digital camera of iPhone5 (8-megapixel, five-element lens with f/2.4 aperture, resolution of 640 × 1136 pixels; Apple Inc., Cupertino, CA, USA) and measured. With the software ImageJ64 1.45c (Wayne Rasband, National Institute of Health, USA, http://imagej.nih.gov/ij Java 1.6.0_65, 64 bit), we measured and compared the typical traits of post-embryonic zebrafish anatomy (Parichy et al., 2009): the standard length (SL), the length between the operculum and caudal peduncle (LOCP) and the height at anterior of anal fin (HAA) (Figure 1).
Results were statistically analyzed with the software GraphPad Prism® 6.0c version, with One-way Analysis of Variance (ANOVA), corrected with Kruskal-Wallis post-test or Dunn's post-test. Mean were considered statistically different when $P < 0.05$.

Figure 1

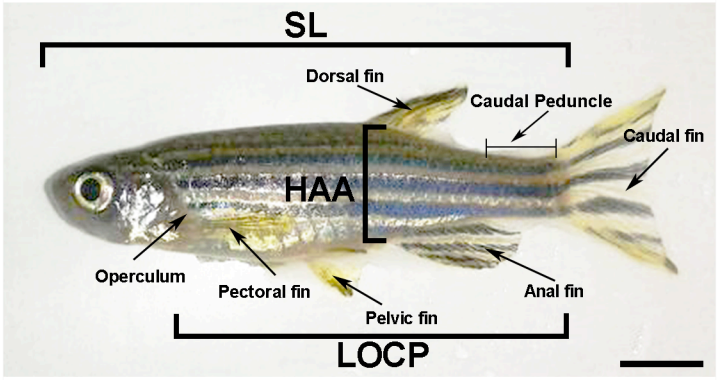

Figure 1: Typical traits of zebrafish externally visible anatomy.
This image shows the typical traits of adult zebrafish anatomy measured to compare wtSod1 and mSod1 transgenic zebrafish with AB zebrafish: the standard length (SL), the length between the operculum and the caudal peduncle (LOCP) and the height at anterior of anal fin (HAA).
Scale bar: 0.5 cm.

4. ADULT ZEBRAFISH SPONTANEOUS LOCOMOTOR ACTIVITY MONITORING

We studied the spontaneous locomotor activity of twelve months old heterozygous wtSod1 and mSod1 zebrafish, and AB zebrafish (Ctrl). For this study, each fish was individually put in a breeding tank (Tecniplast S.p.A, Buguggiate (VA), Italy) of 10.1 cm x 17.4 cm filled with enough water to guarantee an unrestrained swimming of the animal but preventing vertical movements. We recorded the activity of three zebrafish contemporarily, one fish for each genotype and of the same sex, for 10 minutes (Sakowski et al., 2012) with a digital camera (Olympus D755, Olympus Italia Srl, 20090 Opera Zerbo (MI), Italy). The tanks were positioned closed to each other and the lateral walls were darkened in order to avoid that fish movements could be affected by visual cues. The movies were recorded in fish room where light, humidity and temperature are fixed and stable. Each high-resolution movie (xy resolution: 640 x 480 pixels, time resolution: 1 frame every 0.033 s) was acquired in .AVI format, with a fixed camera focus and aperture setting, opened with ImageJ 1.48t (Wayne Rasband, National Institute of Health, USA, http://imagej.nih.gov/ij Java 1.6.0_65, 32-bit), converted in a 8-bit, gray scale image stack and saved as a .TIFF file. The image sequence obtained after this process was cropped in three smaller stacks in order to isolate a single breeding tank and subsequently analyzed to study the motion of one zebrafish at a time.

The analysis of the locomotor activity was then performed with the software Fiji (ImageJ 1.48k, Wayne Rasband, National Institute of Health, USA, http://imagej.nih.gov/ij Java 1.6.0_65, 64-bit) and the MTrack2 Plugin (Zamani et al., 2011). Since the MTrack2 Plugin works on binary files, where the white animal to track moves in a black background, in each stack was properly set a threshold (Image > Adjust > Threshold) in order to specifically isolate the fish (dark in the original file) from the background (bright) and then converted in a binary mask (Process > Binary > Make Binary). The results obtained with the MTrack2 plugin are: an image showing the path followed by the animal and a trackresults.txt file that lists the length of the path and the position of the animal, in x and y coordinates in each image of the stack. For each zebrafish we measured: the distance travelled in the 10 minutes of recording, the time at resting evaluated as the percentage of time at which the distance travelled by the animal was less than 1 pixel (distance *d* was calculated with the formula: $d = \sqrt{(x_2-x_1)^2+(y_2-y_1)^2}$ considering (x_1,y_1) the coordinates of the animal at time 1 and (x_2,y_2) the coordinates of the animal at time 2) and the speed of the animal calculated as the ratio between the total distance travelled by the fish and the time of effective motion obtained subtracting the time spent at resting by the animal from the entire time of locomotor activity monitoring.
Results were obtained in 4 independent experiments with adult zebrafish belonging to two different generations for all the zebrafish lines under investigation. Measures were statistically analyzed with the software GraphPad Prism® 6.0c version, with One-way Analysis of Variance (ANOVA) and corrected with Tuckey multiple comparison procedure. Means were considered statistically different when $P < 0.05$.

5. HISTOLOGICAL ANALYSES

5.1 Adult zebrafish fixation, paraffin embedding and sectioning

Twelve months old wtSod1 and mSod1 heterozygous transgenic zebrafish (generated outcrossing the original wtSod1 and mSod1 transgenic lines with both AB and TL zebrafish) and AB zebrafish (Ctrl) were anaesthetized using 0.6 mM tricaine (ethyl 3-aminobenzoate methanesulphonate, E10521 Sigma-Aldrich®, St. Louis, MO, USA) in fish water (Matthews et al., 2013). The body cavity was opened along the belly and fish were fixed in 10% neutral buffered formalin solution (HT501128, Sigma-Aldrich®, St. Louis, MO, USA) for 24 hours. Animals were decalcified in EDTA acid free 10%, pH 7.2-7.4 (0322, AMRESCO LLC, Solon, OH, USA) for 4 days and then transversely sectioned in 5

segments using fins as standard anatomical references. The first segment (S1) was obtained with a cut in correspondence of the operculum, the second segment (S2) goes from the operculum to the beginning of the pelvic fin, the third segment (S3) spans the pelvic fin till the beginning of the anal fin, the fourth segment (S4) ranges from the beginning to the end of the anal fin and the fifth segment (S5) extends from the end of the anal fin to the caudal peduncle (Figure 2). All the segments were embedded in paraffin with a cranial to caudal orientation, except for the first segment that was embedded with a caudal to rostral orientation. As we decided to focus our attention to the spinal cord we did not analyzed S1 segment containing the brain.

Figure 2

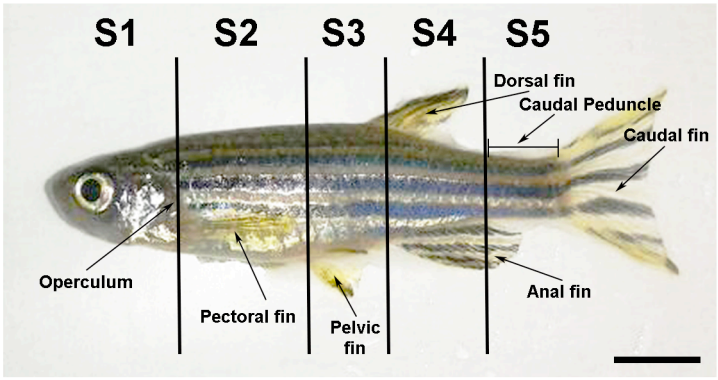

Figure 2: Zebrafish body segmentation used for the histological analyses.
To precisely characterize spinal cord and lateral muscle phenotype of adult wtSod1 and mSod1 zebrafish trunk, we transversely cut each animal in 5 segments using fins (indicated with arrows) as standard anatomical references. Segment 1 (S1) results from a cut in correspondence of the operculum, segment 2 (S2) goes from the operculum to the beginning of the pelvic fin, segment 3 (S3) spans the pelvic fin till the beginning of the anal fin, segment 4 (S4) ranges from the beginning to the end of the anal fin and segment 5 (S5) extends from the end of the anal fin to the caudal peduncle Scale bar: 0.5 cm.

Samples were processed using an automated tissue processor (ASP300, Leica Microsystem, Wetzlar, Germany) and paraffin embedded. Briefly, samples were rinsed in bi-distilled water for 30 minutes, then were gradually dehydrated through an ethanol (02860, Sigma-Aldrich®, St. Louis, MO, USA) series (50%, 70%, 90%, 100%) and xilene (95672, Sigma-Aldrich®, St. Louis, MO, USA) at 37°C and finally embedded in paraffin (327212 Sigma-Aldrich®, St. Louis, MO, USA) at 62°C. Each block, containing all the 5 segments obtained from a fish, was cut in 4 µm sections with a microtome (RM 2255 Leica Biosystems, Nussloch GmbH, Germany) and at least 10 serial sections were collected for each animal and stained with hematoxylin and eosin (at least 3 sections) or processed for immunofluorescence (at least 1 section for each type of immunofluorescence staining and a negative control).

5.2 Hematoxylin and eosin staining

Four µm thickness sections from each sample were stained with hematoxylin and eosin (Mayer's Hematoxylin, C0302; Eosin G, C0362, Diapath S.p.A., Martinengo , BG, Italy) and evaluated under a light microscope (Leica DM750, Leica Microsystem, Wetzlar, Germany). Briefly, the collected sections were deparaffinized in xilene and rehydrated, at room temperature (RT), through a decreasing ethanol series (100%, 95%, 70%) and rinsed in bi-distilled water. The staining consisted in the incubation of sections in hematoxylin for 3 minutes, in the rinsing in running water for 5 minutes and then in the counter-staining with eosin for 3 minutes. Sections were subsequently dehydrated with an ethanol series (95% and 100%) and xylene and mounted with Micromount mounting medium (060200, Diapath S.p.A, Martinengo (BG), Italy).

5.3 Histological analyses of adult zebrafish spinal cord and lateral muscle

Histological sections were visualized with an optical microscope (DM 2500, Leica Microsystem, Wetzlar, Germany) and acquired with a digital camera (DFC310FX, Leica Microsystem, Wetzlar, Germany) associated with the Leica Image Manager Software. For all the animals we acquired, with the 20x objective, one or more partially overlapping images (subsequently fused with the software Fiji and the Plugin Stitching) covering the entire spinal cord and 4 fields containing white muscles fibers for each segment under investigation (S2-S5). All the images acquired were analyzed with the software ImageJ64. In each adult fish, we measured the area of the spinal cord, the number of the spinal motor neurons and the Feret diameter (the longest distance between any two points along the selection boundary drawn around fibers transversally cut) of at least one hundred white muscles fibers, in all the segments of the zebrafish trunk under investigation (S2-S5). Results were statistically analyzed with the software GraphPad Prism® 6.0c version, with Two-way Analysis of Variance (ANOVA) and corrected with Bonferroni post-test. Means were considered statistically different when $P < 0.05$.

5.4 Gfap and Aif1 immunofluorescence staining

Formalin-fixed paraffin-embedded 4 µm sections were deparaffinized in xylene, rehydrated through a graded ethanol series (100%, 95%, 70%) and rinsed in bi-distilled water. Antigen retrieval was performed using citrate buffer pH 6 1x (T0050, Diapath S.p.A, Martinengo (BG), Italy) in a pressure cooker (2100-Retriever, Electron Microscopy Sciences, Hatfield, PA, USA). Slides were rinsed and treated with PBS 1x (137 mM NaCl, 2.7 mM KCl, 10 mM Na_2HPO_4, 2 mM KH_2PO_4) containing 10% normal goat serum (Diapath S.p.A, Martinengo (BG), Italy) for 30 minutes, to reduce non-specific background staining, and then incubated for 1 hour at RT with the following primary antibodies: rabbit polyclonal anti-Gfap (glial fibrillary acidic protein, an astrocytes marker) 1:500 (Z0334, Dako, Glostrup, Denmark) and rabbit polyclonal anti-Aif1 (allograft inflammatory factor 1, a marker of activated macrophages and neutrophils) 1:500 (019-19741, Wako Pure Chemical Industries, Ltd, Osaka, Japan). Secondary antibody: AlexaFluor® 488 F(ab')2 Fragment of Goat Anti-Rabbit IgG (H+L) (A11070, Molecular Probes®, Life Technologies Europe BV, Monza (MB), Italy) for both sections incubated with anti-Gfap and anti-Aif1 was then added for 30 minutes. Negative immunohistochemical controls for each sample were prepared by replacing the primary antibody with PBS 1x containing 10% normal goat or rabbit serum. Known positive control sections were included in each immunolabelling assay.

5.5 Images acquisition

The immunofluorescence stained sections were acquired at the confocal microscope TCS SP5 (Leica Microsystems, Wetzlar, Germany) with a 40x oil-immersion objective, 8-bit gray-scale, opened pinhole: 3 airy units, 3 frames averaging, scan speed 400 Hz, format: 1024 x 1024). We set the zoom at 1 in order to acquire the entire section of the spinal cord in a single image (pixel size: 378 nm) and the zoom at 2 to acquire fields of the lateral muscle (pixel size: 189 nm) to adequately visualize the inflammatory cells. We acquired 3 fields of white muscle fibers for each segment analyzed (S2-S5). To excite AlexaFluor® 488 we used the laser line with a wavelength of 488 nm and we collected the light emitted setting the photomultiplier (PMT) bandwidth between 498 and 550 nm.

5.6 Evaluation of reactive astrogliosis and microgliosis in the spinal cord and inflammatory infiltrate in the lateral muscle

The fluorescence images collected were analyzed with the software ImageJ64. In each zebrafish segment under investigation (S2-S5), we measured the ratio between the mean fluorescence intensity signal (in arbitrary units a.u.) in the spinal cord and the area of the same spinal cord section (in μm^2) for both Gfap and Aif1 staining. To quantitatively evaluate the inflammatory infiltrate in the zebrafish lateral muscle we measured both the ratio between the surface occupied by the fluorescence signal and the total area under investigation and the ratio between the number of Aif1 positive cells and the total area analyzed. The identification of Aif1 positive cells was obtained first, through the generation of a binary mask for each fluorescence image using the Image > Adjust > Threshold function of ImageJ in order to specifically isolate the signal associated to the inflammatory cells from the background and then using the function Process > Binary > Make Binary to produce a binary mask where fluorescent cells result black in a white background. With the function Analyze > Analyze Particles we selected the area occupied by each cell setting a dimensional threshold (we identified as signal associated to cells only areas whose dimensions were higher than 0.1 μm^2). The count of the number of the identified particles gave us the information regarding the number of cells in the area and thanks to the Analyze > Measure function we obtained the measure of the area occupied by the inflammatory cells and the mean fluorescence intensity associated.
Results were statistically analyzed with the software GraphPad Prism® 6.0c version, with Two-way Analysis of Variance (ANOVA), corrected with Bonferroni post-test. Means were considered statistically different when $P < 0.05$.

6. ADULT ZEBRAFISH SNAP-FREEZING AND FLUORESCENCE STAINING OF CRYOSTAT SECTIONS

Adult mSod1 heterozygous zebrafish and AB zebrafish (Ctrl) were anesthetized with 0.6 mM tricaine methane sulphonate in fish water (Matthews et al., 2013). Under the stereomicroscope (Leica S6D and Leica L2 optic fibers, Leica Microsystem, Wetzlar, Germany), the head of the fish was removed by cutting at the level of the operculum and discarded while, the remaining trunk of the fish was transversally cut in correspondence of the pelvic fin. The two segments obtained were embedded together in Optimal Cutting

Temperature (OCT, Tissue-tek®, Sakura Finetek Europe B.V. KvK, Leiden, The Netherlands) with a rostral to caudal orientation and snap-frozen in liquid nitrogen. The frozen blocks were cut with a cryostat (Reichert-Jung 2700-frigocut, Buffalo, NY, USA) in transversal sections of 20 µm each, collected on a glass slide and covered with PBS 1x. Sections were fixed with 2% paraformaldehyde (19200, Electron Microscopy Sciences Hatfield, PA, USA) in PBS 1x for 15 minutes at RT, then permeabilized with PBS-TT (PBS 1x, 0.2% TWEEN®20 (P9416, Sigma-Aldrich®, St. Louis, MO, USA), 0.2% Triton™ X-100 (T8787, Sigma-Aldrich®, St. Louis, MO, USA)) and incubated at RT for 30 minutes in blocking solution: 3% Bovine Serum Albumine (BSA, A7906 Sigma-Aldrich®, St. Louis, MO, USA) in PBS-TT. Sections were incubated at RT for two hours with the primary antibody: rabbit polyclonal antibody anti-SV2A (synaptic vesicle glycoprotein 2A) staining synaptic vesicles in the presynaptic terminal (HPA007863, Sigma-Aldrich®,St. Louis, MO, USA) 1:1000 in blocking solution. After rinsing with PBS-TT, sections were incubated at RT for 1 hour with the secondary antibody: AlexaFluor® 488 F(ab')2 Fragment of Goat Anti-Rabbit IgG (H+L)) 1:200 and α-Bungarotoxin-Alexa Fluor® 555 conjugate 1:500 (B35451, Molecular Probes®, Life Technologies Europe BV, Monza (MB), Italy) in blocking solution. After rinsing with PBS-TT, stained sections were mounted in ProLong® Gold antifade reagent and mounting medium (P36934, Molecular Probes®, Life Technologies Europe BV, Monza (MB), Italy) and stored at 4°C in the dark. Negative controls for each sample were prepared by replacing the primary antibody solution with blocking solution.

Samples were acquired with the confocal microscope TCS SP5 with 63x oil-immersion objective, 2.5 zoom. We used the laser line at 488 nm to excite AlexaFluor® 488 and we detected the wavelengths emitted between 498 nm and 540 nm. We excited α-Bungarotoxin-Alexa Fluor® 555 with the laser line at 561 nm and we collected the light emitted setting the collecting window of the PMT between 570 nm and 750 nm. For each sample we acquired z-stacks containing the entire depth of the cryostat section with z-step size of 0.25 µm. For each animal we collected 10-15 fields of 98.41 µm x 98.41 µm (pixel size: 96.10 nm, format 1024 x 1024) of the lateral white muscle of the trunk, containing from 7 to 13 neuromuscular junctions.

6.1 Analyses of the percentage of innervation of zebrafish lateral muscle and density and dimension of neuromuscular junctions pre- and post-synaptic clusters

The z-stacks acquired were analyzed with the software ImageJ64. We evaluated the percentage of innervation of white fibers in the lateral muscles of the adult zebrafish trunk and the density and dimension of neuromuscular junctions pre- and post-synaptic clusters. For each animal, we analyzed at least 100 neuromuscular junctions found in sections belonging to both embedded segments of the trunk.

The percentage of innervation was established first, generating a maximum projection (Image > Stack > Z-Project -maximum intensity mode-) of both SV2A and α-Bungarotoxin (α-Btx) channels (the z-stacks were previously filtered with the Mean filter set at 0.5 to reduce fluorescence noise) and then producing a merge (Image > Color > Merge Channels) of the two channels. In the merged image we counted the total number of neuromuscular junctions, the number of post-synaptic clusters facing pre-synaptic clusters in each field and subsequently the percentage of innervation and the density of pre- and post-synaptic specializations.

The measure of the dimensions of neuromuscular junctions pre- and post-synaptic clusters was obtained, for each z-stack acquired, first, through the generation of a binary mask from the maximum projection of SV2A and α-Btx using the Image > Adjust > Threshold function in order to specifically identify the signal associated to the synaptic vesicles, in the pre-synapse, and of acetylcholine receptors clusters, in the post-synaptic terminal, from the background. Then, using the function Process > Binary > Make binary we produced a binary mask where the fluorescence signal results black in a white background. With the function Analyze > Analyze Particles we selected the area occupied by the clusters setting a dimensional threshold (we identified as signal associated to clusters only areas whose dimensions were higher than 0.1 μm^2). The count of the number of the identified particles gave us the information regarding the density of SV2A and α-Btx clusters in the field analyzed and thanks to the Analyze > Measure function we obtained the measure of the area of each cluster and the mean fluorescence intensity associated. Results were statistically analyzed with the software GraphPad Prism® 6.0c version, with the unpaired Student t test. Means were considered statistically different when $P < 0.05$.

7. ELECTRON MICROSCOPY

7.1 Adult zebrafish lateral muscle and whole zebrafish embryos and larvae preparation for electron microscopy

Twelve months old wtSod1 and mSod1 heterozygous transgenic zebrafish and AB zebrafish (Ctrl) were anaesthetized using 0.6 mM tricaine in fish water (Matthews et al., 2013). Animals were rapidly sectioned in 5 segments using fins as standard anatomical references, as it was previously described (see the detailed description in paragraph 5 and Figure 2), and each segment was independently fixed in 3% glutaraldehyde (16220, Electron Microscopy Sciences Hatfield, PA, USA), 2% paraformaldehyde in 0.05 M sodium cacodylate (12300, Electron Microscopy Sciences Hatfield, PA, USA) buffer with 1% sucrose (21600, Electron Microscopy Sciences Hatfield, PA, USA) and 1 mM magnesium sulfate (M7506, Sigma-Aldrich®,St. Louis, MO, USA), for 2 hours at RT. Subsequently, under a stereomicroscope, the lateral muscle of each segment was dissected in small pieces of 1 mm x 1 mm and further fixed in the same fixative solution for 48 hours at 4°C. Samples were rinsed 3 times for 10 minutes with sodium cacodylate buffer 0.1 M, post-fixed in 2% osmium tetroxide (19150, Electron Microscopy Sciences Hatfield, PA, USA) in 0.1 M cacodylate buffer for 1 hour. After multiple rinses with 0.1 M cacodylate buffer and bi-distilled water, samples were counter-stained with a saturated solution of uranyl acetate (73943, Sigma-Aldrich®, St. Louis, MO, USA) in 20% ethanol for 45 minutes in the dark. After rinsing with 20% ethanol, samples were gradually dehydrated with an ethanol series (70%, 80%, 90%, 100%) and propylene-oxide (110205, Sigma-Aldrich®, St. Louis, MO, USA). Meanwhile, Epon-Spurr resin was prepared mixing Epon and Spurr resins 1:1. Epon (18010, Eponate 12 kit (DMP30 catalyst), TED PELLA Inc., Redding, CA, USA) was prepared mixing properly dodecenylsuccinic anhydride (DDSA), methyl nadic anhydride (MNA), Epon 812 and Epon Accelerator DMP30, while Spurr (18300-4221, Low Viscosity "Spurr" Kit, TED PELLA Inc., Redding, CA, USA) component was prepared mixing vinylcyclohexene dioxide (VCD), diglycidyl ether of polypropylene glycol (DER), nonenyl succinic anhydride (NSA) and dimethylaminoethanol (DMAE) according to manufacturers specifications. Samples were gradually infiltrated first with a mixture of Epon-Spurr and propylene-oxide 1:1 for 12 hours, then with Epon-Spurr and propylene-oxide 2:1 for 3 hours and eventually put in pure resin before polymerization at 60°C for 48 hours.

Whole zebrafish embryos at 24 and 48 hpf and larvae at 4 dpf were fixed in 2% glutaraldehyde and 2% paraformaldehyde in 0.1 M sodium cacodylate buffer for 12 hours at 4°C and then processed following the same protocol describe above.

7.2 Ultra-thin sections preparation and samples observation at the transmission electron microscope

Resin embedded samples were cut with the ultramicrotome (Leica EM UC6, Leica Microsystem, Wetzlar, Germany) in semi-thin sections of 0.5 µm thickness with a glass knife, gathered and stained with 0.1% toluidine blue (22050, Electron Microscopy Sciences Hatfield, PA, USA) and 0.1% methylene blue (18600, Electron Microscopy Sciences Hatfield, PA, USA) in 0.1 M sodium phosphate buffer and observed at the optical microscope (Leica DM2500, Leica Microsystem, Wetzlar, Germany) to identify the region of the sample to investigate at the ultrastructural level. Then, ultra-thin sections of 70 nm were cut with a diamond knife (Ultra 45°, DiATOME, 2501 Biel, Switzerland) and collected on copper grids (G300-Cu, Electron Microscopy Sciences Hatfield, PA, USA) and counter-stained with uranyl acetate solution for 20 minutes and 1% lead citrate (17800, Electron Microscopy Sciences Hatfield, PA, USA) for 7 minutes. Samples were observed at the transmission electron microscope (TEM) (Philips CM10, 5656 AE, Eindhoven, The Netherlands) at 80 kV and images were acquired with a digital camera (Morada, Olympus, Münster, Germany).

7.3 Ultrastructural analyses of neuromuscular junctions and muscles of zebrafish

We performed qualitative ultrastructural analyses of adult zebrafish neuromuscular junctions and muscles in search of ultrastructural alterations associated to the pathology. We performed the quantitative ultrastructural analyses of adult zebrafish muscular mitochondria in the lateral muscles of the S4 and S5 segment of the trunk. We measured, on electron micrographs acquired at 10500x and 13500x (format 3708 x 2627 pixels, pixel size: 3.5 nm and 2.9 nm, respectively), area, perimeter and circularity of about 100 mitochondria in each animal, with the software ImageJ64. Results were statistically analyzed with the software GraphPad Prism® 6.0c version, with One-way Analysis of

Variance (ANOVA), corrected with Tuckey post-test. Means were considered statistically different when $P < 0.05$.

In zebrafish larvae at 96 hpf we performed morphological and morphometric analyses of neuromuscular junctions with the software ImageJ64. To this aim, we acquired electron micrographs at 34000x (format 3708 x 2627 pixels, pixel size: 1.03 nm) of the muscle of zebrafish larvae trunk. In each neuromuscular junction profile we evaluated synaptic boutons area, synaptic vesicles number, density, and distribution and mitochondria number and morphological features. We measured area, perimeter and circularity for both synaptic vesicles and mitochondria in the neuromuscular junctions (Cappello et al., 2012). The ultrastructural analysis of zebrafish larvae muscles was performed on electron micrographs acquired at 10500x and 13500x (format 3708 x 2627 pixels, pixel size: 3.5 nm and 2.9 nm, respectively). We measured sarcomeres length as the distance between two consecutive H-bands in approximately 100 sarcomeres in each animal. On the same micrographs, we performed the ultrastructural analysis of muscular mitochondria measuring area, perimeter and circularity of about 100 mitochondria in each animal. Results were statistically analyzed with the software GraphPad Prism® 6.0c version, with One-way Analysis of Variance (ANOVA), corrected with Tuckey post-test. Mean were considered statistically different when $P < 0.05$.

8. WHOLE-MOUNT IMMUNOFLUORESCENCE STAINING OF ZEBRAFISH EMBRYOS AND LARVAE

Zebrafish embryos at 24 and 48 hpf and larvae at 96 hpf were fixed with 4% paraformaldehyde and 1% DMSO (D2438, Sigma-Aldrich®,St. Louis, MO, USA) in PBS 1x, for 2 hours at RT and then over night at 4°C. After rinsing with PBS 1x, fish were treated with 1 mg/ml collagenase (C9891, Sigma-Aldrich®, St. Louis, MO, USA) for 7, 15 and 90 minutes respectively at RT and incubated for at least 12 hours at 4°C with α-Bungarotoxin-AlexaFluor® 555 1:100 in 3% BSA and PBS-TT (Panzer et al., 2005). After rinsing with PBS 1x, samples were incubated in acetone (650501, Sigma-Aldrich®, St. Louis, MO, USA) at -20°C for 30 minutes, permeabilized with 4 washes in PBS-TT of 5 minutes each, post-fixed with 4% paraformaldehyde in PBS 1x at RT and then quenched with 50 mM NH_4Cl (A9434, Sigma-Aldrich®, St. Louis, MO, USA). Samples were permeabilized 3 x 10 minutes with PBS-TT and after an incubation of 3 hours in blocking solution (3% BSA in

PBS-TT) samples were incubated with primary antibodies: rabbit polyclonal anti-SV2A 1:200 and mouse monoclonal anti-acetylated tubulin (T7451, Sigma-Aldrich®, St. Louis, MO, USA) 1:500 in blocking solution over night at 4°C. The following day fish were washed 4 x 1 hour in PBS-TT and then incubated with secondary antibodies: AlexaFluor® 488 F(ab')2 Fragment of Goat Anti-Rabbit IgG (H+L) 1:200 and Alexa Fluor® 633 F(ab′)2 Fragment of Goat Anti-Mouse IgG (H+L) 1:200 (A21053, Molecular Probes®, Life Technologies Europe BV, Monza (MB), Italy) over night at 4°C. Then samples were washed with PBS 1x and stored at 4°C in the dark.

8.1 Confocal images acquisition of zebrafish embryos and larvae

Zebrafish embryos and larvae were mounted in 1% Low Melting Point Agarose (A9414, Sigma-Aldrich®, St. Louis, MO, USA) in PBS 1x onto the glass of a 35 mm imaging dish with a glass bottom (81156, Ibidi®, Planegg/Martinsried, Germany) and properly oriented in order to obtain a lateral view of the trunk.

Confocal images were acquired with the confocal microscope Leica TCS SP5. Since the development and maturation of the motor system occurs following a rostral to caudal wave, we acquired z-stacks of selected regions of the trunk to assure the morphological comparison of homogenously developed structures (both spinal motor nerves and neuromuscular junctions). At 24 hpf, we acquired the region of the trunk ranging from the 12th and the 16th somite above the yolk tube and then the immediately subsequent region included by the 17th and 21st somite; at 48 hpf, we acquired z-stacks of the trunk comprised by the 9th and the 13th somite, above the yolk tube; while at 96 hpf, we acquired the portion of the trunk contained by the 10th an the 15th somite.

We acquired z-stacks using a 20x objective, 0.7 numerical aperture (NA), and 2.5 zoom. This allowed us to acquire z-stacks of 310 µm x 310 µm fields (1024 x 1024 image format, pixel size of 303 nm x 303 nm) with a z-step size of 0.84 µm. We excited: AlexaFluor® 488 with the laser line at 488 nm, setting the PMT wavelengths collecting window between 500 nm and 555 nm, AlexaFluor® 555 with the 561 nm laser line and we collected emitted wavelengths between 571 nm and 650 nm and we excited AlexaFluor® 633 with the 633 nm laser and setting the PMT collecting bandwidth between 643 nm and 750 nm. We used the bidirectional scanning mode acquisition; we set the pinhole at 1 airy unit and averaged each channel acquired with 3 lines averaging.

8.2 Second Harmonic Generation (SHG) Signal detection - fiber caliber and sarcomeres length measurement

Second-harmonic generation (SHG) is a nonlinear optical process arising from the interaction of light with polarizable materials lacking centrosymmetry. The highly ordered arrangements of myosin filaments in muscle fibers is a perfect source for the generation of this process, therefore the detection of the SHG signal generated by myosin filaments represents an ideal tool to investigate muscle fibers fine structure and associated alterations. This technique, in fact, exploits intrinsic properties of proteins peculiarly arranged in tissues, allowing imaging of intact tissues or living organisms without labeling and the use of non-linear near infrared excitation, minimizes autofluorescence background and enables direct optical sectioning (Huang et al., 2011).

The SHG signal detection was performed on zebrafish larvae at 96 hpf stained and mounted as described in the previous paragraph. The signal was detected with a confocal microscope Leica TCS SP5 equipped with a multi-photon excitation setup. In this case, AlexaFluor® 488 and AlexaFluor® 633 were simultaneously acquired exciting the former with the laser line at 488 nm and the latter with the 633 nm laser and setting the PMTs wavelengths collecting windows between 500 nm and 555 nm and between 643 nm and 750 nm, respectively. AlexaFluor® 555 was separately excited with the 561 nm laser line and emitted wavelengths were collected between 571 nm and 650 nm. SHG signal was detected exciting the samples with a tunable pulsed infrared Ti:Sapphire laser (Chameleon™ Ultra family, Coherent®, Milano, Italy) with a wavelength of 900 nm and collecting the signal with an opened pinhole (600 µm) setting the PMT bandwidth between 380 nm and 400 nm. We averaged the signal setting the line average at 3. We acquired z-stacks of each channel, in the order described above, using the stack-by-stack mode, using a 20x objective, 0.7 numerical aperture (NA), and 2.5 zoom. This allowed us to acquire z-stacks of 310 µm x 310 µm fields (1024 x 1024 image format, pixel size of 303 nm x 303 nm) with a z-step size of 0.84 µm.

The evaluation of the mean fiber caliber of Ctrl, wtSod1 and mSod1 zebrafish larvae was performed in 30 to 60 randomly selected fibers running along the entire stack while the length of sarcomeres was calculated as the distance between two minima in the intensity plot profile (Analyze > Plot profile) obtained tracing a line perpendicularly to the main axis of the fiber (measuring from 29 to 60 sarcomeres in several fibers).

Measures were statistically analyzed with the software GraphPad Prism® 6.0c version, with One-way Analysis of Variance (ANOVA) corrected with Tuckey or Kruskall-Wallis multiple comparison procedure. Means were considered statistically different when $P < 0.05$.

8.3 Analysis of the length and axonal branches of spinal motor nerves in zebrafish embryos 24 and 48 hpf

The evaluation of the length, of the unbranched axonal length (UAL) and of the number of branches of motor nerves in zebrafish embryos at 24 hpf (Kabashi et al., 2010 and 2011) was performed with the software ImageJ64 on maximum projections of the SV2A channel; in fact, at this stage of development the signal of acetylated tubulin along the axons is too dim to allow a precise morphological evaluation; on the contrary, synaptic vesicles, travelling along the entire length of the growing axons, generate a bright signal that perfectly traces the path followed by nerves. We analyzed the morphological features of motor nerves in 2 portions of the trunk: the first included by the 12^{th} and the 16^{th} somite and the second comprised by the 17^{th} and the 21^{st} somite.

In zebrafish embryos at 48 hpf synaptic vesicles are already clustered at motor axons terminals therefore, the measurement of the parameters described before cannot be performed only on the maximum projection obtained from the SV2A z-stacks. In this case, we used ImageJ64 to generate a merge of the maximum projections obtained from both SV2A and AcTub z-stacks. The AcTub signal was used to trace the path followed by motor axons and SV2A to easily visualize nerves endings and identify axonal branches in the portion of the trunk included by the 9^{th} and 13^{th} somite.

Results were statistically analyzed with the software GraphPad Prism® 6.0c version, with One-way Analysis of Variance (ANOVA), corrected with Tuckey post-test. Means were considered statistically different when $P < 0.05$.

8.4 3D-colocalization and synaptic vesicles and AChRs clusters dimension analyses at early developmental stages

The evaluation of the developmental degree of neuromuscular junctions in Ctrl, wtSod1 and mSod1 zebrafish embryos at 48 hpf and larvae at 96 hpf was performed with a three-dimensional colocalization analysis. With the ImageJ64 Plugin JACoP, we performed an object-based colocalization analysis (Bolte & Cordelières, 2006) that allowed

the measurement of synaptic vesicles and AChRs clusters density in zebrafish embryos and larvae muscles and, among them, the percentage of SV2A and AChRs colocalizing clusters. For both 48 hpf and 96 hpf zebrafish, we first cropped both SV2A and AChRs stacks in order to isolate a portion of the volume acquired comprising the muscle of the animal (in the case of larvae at 96 hpf we were helped by SHG myosin signal). In the cropped stacks obtained, we removed the fluorescence signal due to the developing sensory system with the Edit > Clear function and then we applied a 0.5 Mean filter to remove noise. We then opened SV2A stack as channel A and AChRs stack as channel B with JACoP, we set proper fluorescence intensity threshold for both channels and a dimensional threshold (we took under consideration only clusters whose dimensions were bigger than 0.1 μm^2) to specifically identify clusters and then we performed an object-based colocalization analysis working on centers-particles coincidence, where cluster centers were identified as the centers of mass. The mean dimension of SV2A and AChRs clusters was calculated on the cropped stacks. First, with the function Image > Adjust > Threshold we generated a binary stack of each channel using the same threshold used for the colocalization analysis, and then with the function Analyze > Analyze particles we measured the dimension of each cluster in the stack.
Results were statistically analyzed with the software GraphPad Prism® 6.0c version, with One-way Analysis of Variance (ANOVA), corrected with Tuckey post-test. Means were considered statistically different when $P < 0.05$.

9. BEHAVIORAL TESTS ON ZEBRAFISH EMBRYOS AND LARVAE

One of the advantages of zebrafish as a model for the study of locomotor network development is that the progressive organization of neural circuits is associated to the appearance of stereotypic motor activity that includes three sequentially appearing behaviors: a transient period of alternating tail coilings, followed by the response to touch and the appearance of organized swimming (Brustein et al., 2003). We therefore decided to exploit this advantage to test if the expression of the different forms of Sod1 affects Ctrl, wtSod1 and mSod1 zebrafish motor responses. We focused our attention on spontaneous coiling at 20 hpf, embryonic movements consisting in a full body contraction that brings the tip of the tail to the head; the touch evoked coiling response at 48 hpf, phenotype evoked by the touch in an embryo, which responds with fast coiling of the trunk bending over the head, arising when the sensory system integrates and drives motor responses and finally

touched evoked burst swimming at 96 hpf: a fast forward swim with large bend angles, maximally at mid-body, of larval zebrafish (Kalueff et al., 2013).

9.1 Spontaneous tail coilings analysis

Spontaneous coiling behavior was evaluated in embryos at 20 hpf. Each embryo was tested for the lack of touch evoked coiling response with a gentle sensory stimulation before proceeding with the behavioral test. Five embryos at a time were dechorionated, and singularly transferred in fish water in a 3.5 mm round petri dish where 5 niches were engraved to host them. Tail coilings were detected at RT with a 5 minutes movie (time resolution of 45 frames/s), obtained with the Leica Digital Camera DCF480 mounted on the stereomicroscope Leica MZFLIII, magnification 2.5x associated with the Leica Application Suite (LAS) software (Leica Microsystem, Wetzlar, Germany). For each embryo, we evaluated the frequency of spontaneous tail coilings, the percentage of multiple or complex coilings, that are the percentage of coilings consisting in two or more repeated bends of the trunk before returning to the resting condition and the relative percentage of multiple/complex coilings consisting in alternated left-right bends of the entire body or in tail bends on the same side of the body. To test the effect of riluzole (2-Amino-6-(trifluoromethoxy) benzothiazole, R116, Sigma-Aldrich®, St. Louis, MO, USA) or vehicle (DMSO, riluzole solvent) on spontaneous tail coilings we gently removed fish water in order to keep embryos in the same position and we added fish water containing 5 μM riluzole or 0.2% DMSO. After 5 minutes we recorded another 5 minutes movie and performed the same analyses. Results were statistically analyzed with the software GraphPad Prism® 6.0c version, with One-way Analysis of Variance (ANOVA), corrected with Tuckey post-test or unpaired Student t test. Means were considered statistically different when $P < 0.05$.

9.2 Touch evoked coiling response analysis

Ctrl, wtSod1 or mSod1 zebrafish embryos at 48 hpf, placed in 1% low melting-point-agarose in fish water at 37°C, were transferred in a 10 mm round petri dish in a drop of agarose and oriented with the dorsal side up with the belly facing the bottom of the petri dish. When the agarose solidified, we gently removed all the agarose behind the yolk ball and we added a drop of water on the top of the fish. At least 5 tail coilings were evoked

touching the trunk of the embryo above the yolk ball with the tip of a microloader. Touch evoked tail coilings were recorded at RT with a movie file (time resolution of 45 frames/s), obtained with the Leica Digital Camera DCF480 mounted on the stereomicroscope Leica MZFLIII, magnification 1.6x associated with the Leica Application Suite (LAS) software (Leica Microsystem, Wetzlar, Germany). For each embryo we measured the duration of the response and the angle of maximum amplitude of tail flexion with the software ImageJ. Measures were statistically analyzed with the software GraphPad Prism® 6.0c version, with One-way Analysis of Variance (ANOVA) corrected with Tuckey multiple comparison procedure. Means were considered statistically different when $P < 0.05$.

9.3 Touch evoked burst swimming analysis

Zebrafish larvae at 96 hpf were individually transferred in a 10 mm petri dish placed on a mesh of 0.5 x 0.5 cm squares at RT. Burst swimming responses were evoked touching the trunk of the embryo behind the head with the tip of a microloader and recorded with high resolution movies obtained with the digital camera of iPhone5 (8-megapixel, five-element lens with f/2.4 aperture, resolution of 640 × 1136 pixels; Apple Inc., Cupertino, CA, USA). For each embryo we measured the duration of the response and the distance swum in at least 5 responses.
Results were statistically analyzed with the software GraphPad Prism® 6.0c version, with One-way Analysis of Variance (ANOVA) corrected with Tuckey multiple comparison procedure. Means were considered statistically different when $P < 0.05$.

10. EXPERIMENTAL PROCEDURE FOR THE CORRELATION OF EMBRYOS BEHAVIOR AT 20 hpf AND SPINAL NERVES MORPHOLOGY AT 24 hpf

Although the identification of wtSod1 and mSod1 embryos at 48 hpf and larvae at 96 hpf, obtained intercrossing adult heterozygous mSod1 and wtSod1 transgenic fish, is very simple thanks to the expression of the fluorescent protein DsRed in all tissues, after heat-shocking embryos at 24 hpf for 1 hour at 37°C; it is impossible to screen transgenic embryos before 48 hpf for two main reasons: first, the heat-shock before 24 hpf is lethal for most embryos and second, after the temperature shock, the expression of a detectable fluorescence signal in tissues requires several hours. For these reasons, we developed an

experimental procedure that, not only allowed us the identification of wtSod1 and mSod1 transgenic embryos at 20 hpf but also the correlation of the aberrant motor phenotype with the morphology of the spinal nerves at 24 hpf (Figure 3).

Zebrafish embryos at 20 hpf, obtained intercrossing heterozygous wtSod1 or mSod1 transgenic fish (Figure 3,A), were dechorionated and then positioned in a 3.5 mm petri dish where 5 niches were engraved to host individual embryos (Figure 3,B). Embryos were tested for their spontaneous tail coilings phenotype first in fish water alone and then, after 5 minutes of its substitution, with fish water containing 5 µM riluzole or 0.2% DMSO paying attention at keeping all the embryos in the same niche in the dish. At the end of the test, each fish was individually put in a 0.5 ml Eppendorf tube in fish water. At 24 hpf, embryos were fixed in 4% paraformaldehyde in PBS 1x over night at 4°C and singularly processed for immunofluorescence staining as previously described in chapter 8. After image acquisition at the confocal microscope each embryo was gently collected from agarose and individually placed in a 1.5 ml Eppendorf tube for DNA extraction.

The DNA was extracted employing the salting out protocol: each embryo has been incubated with 200 µl of salting out digestion buffer containing 10 mM NaCl, 10 mM TRIS HCl (T5941, Sigma-Aldrich®,St. Louis, MO, USA) pH 8.1, 10 mM EDTA (E6758, Sigma-Aldrich®,St. Louis, MO, USA) pH 8, 0.5% Sodium Dodecil Sulfate (SDS, L3771, Sigma-Aldrich®,St. Louis, MO, USA) 10 mg/ml proteinase K (P4850, Sigma-Aldrich®,St. Louis, MO, USA) over night at 55°C. Then 20 µl of 3 M Sodium Acetate (71196, Sigma-Aldrich®,St. Louis, MO, USA) pH 5.2 and 600 µl of absolute ethanol (02860, Sigma-Aldrich®,St. Louis, MO, USA) have been added. After 1 hour at -80°C, samples were centrifuged at 13000 rpm at 4°C for 30 minutes, supernatant was discarded and each pellet was dried at 55°C. The precipitated DNA was resuspended in 50 µl bi-distilled water at 80°C for 15 minutes. The wtSod1 and mSod1 transgenic embryos were identified by PCR using a pair of primers (Sigma-Aldrich®, St. Louis, MO, USA) spanning a 200 bp region of the DsRed ORF (DsRedFF: 5'-GTAATGCAGAAGAAGACTATGGGCTGGGAG-3'; DsRedRR: 5'-A TGTCCAGCTTGGAGTCCACGTAGTAGTAG-3'). The presence of DNA in each sample was checked by PCR with primers specifically amplifying the 18S ribosomal subunit DNA (18S_sense 5'-ACCTCACTAAACCATCCAATC-3'; 18S_antisense 5'-AGGAATTCCCAGTAAGCGCA-3'.). To exclude contaminations a PCR negative control without template has been always run in parallel to the DNA samples. The PCRs were performed using the Mastermix GoTaq® G2 master (M782A, Promega Italia Srl, Milano, Italy), with 0.4 µM of each primer following the PCR two-step protocol: 2 minutes of

denaturation at 95°C, then 35 cycles consisting of 15 seconds of denaturation (92°C) and 30 seconds of primers annealing and elongation (55°C).

Figure 3

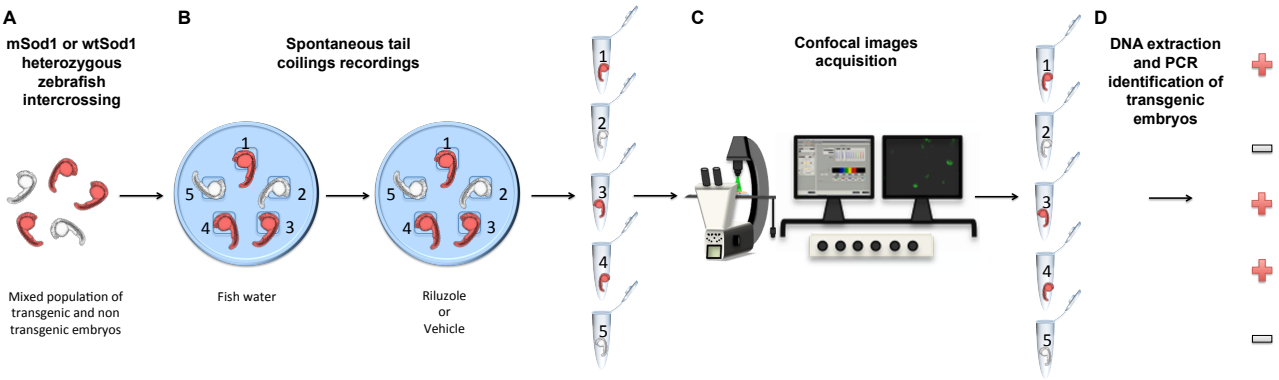

Figure 3: Flow chart showing the protocol followed to correlate embryos behavioural response at 20 hpf and spinal nerves morphology at 24 hpf.
Heterozygous mSod1 and wtSod1 mating generates a mixed population of transgenic and non-transgenic embryos that cannot be distinguished thanks to DsRed expression (A). We performed spontaneous tail coilings analyses placing embryos in the niches engraved in a petri dish paying attention to carefully removing fish water and adding riluzole or vehicle solution without displacing the embryos from their position (B). At the end of the experiment, each fish was individually transferred in a tube, fixed and stained for immunofluorescence and then visualized at the confocal microscope (C). When the images acquisition was completed, each fish was singularly collected in a tube, its DNA was extracted and with PCR transgenic fish were identified thanks to the gene encoding the protein DsRed (D).

11. MEMBRANE VOLTAGE MEASUREMENT OF ZEBRAFISH EMBRYOS SPINAL NEURONS USING THE FRET-BASED VOLTAGE BIOSENSOR MERMAID

To test whether the aberrant behavioral phenotype observed in mSod1 embryos at 20 hpf, was associated to alteration in the spontaneous depolarizations of spinal neurons, in the intact spinal network of living embryos, we used the fluorescence resonance energy transfer (FRET) based voltage biosensor Mermaid (Tsutsui et al., 2008). This biosensor is a chimeric protein generated fusing the voltage-sensing domain (VSD) of the non-ion channel protein, *Ciona intestinalis* voltage sensor–containing phosphatase (Ci-VSP) with two fluorescent proteins, as donor and acceptor pair. The donor of the FRET pair is a monomeric variant of the green-emitting fluorescent protein derived from the soft coral Umi-Kinoko (*Sarcophyton sp.*), mUKG. This protein has a 483 nm absorption peak (molar extinction coefficient, ε = 60,000 M^{-1} cm^{-1}) and a 499 nm emission peak (a fluorescence

quantum yield, QY of 0.72). The QY is fairly constant over a wide pH range, and it has a relatively low pKa of 5.2. The acceptor of the FRET pair is a faster-maturating monomeric version of the orange-emitting fluorescent protein Kusabira Orange, mKO_k. This fluorescent protein has a 551 nm absorption peak (ε = 105,000 M^{-1} cm^{-1}) and a 563 nm emission peak (QY = 0.61) and is fairly pH-resistant (pKa = 4.2). The mUKG's emission and mKO_k's absorption spectra are greatly overlapping with a calculated Förster distance of 5.5 nm. This biosensor thanks to the domain of Ci-VSP is efficiently localized at the plasmamembrane, it displays ~40% changes in emission ratio per 100 mV, allowing for direct visualization of electrical activities in cultured excitable cells, it has fast on-off kinetics at warm (33 °C) temperatures and can report voltage spikes comparable to action potentials, it is resistant to pH changes occurring during neuronal activity and it has been efficiently expressed and proven to be functional in zebrafish myocardial cells (Tsutsui et al., 2010).

11.1 pHuC_Mermaid vector generation

The FRET-based voltage biosensor Mermaid, cloned in the pCS4+ vector (see Map in Figure 4), was gently provided by Dr. Hideaki Tsutsui (Laboratory for Cell Function Dynamics, Brain Science Institute, RIKEN, 2-1 Hirosawa, Saitama 351-0198, Japan). In order to obtain neuronal specific expression of the biosensor, the Mermaid ORF (Open Reading Frame) has been cloned under the zebrafish HuC pan neural promoter (Park et al., 2000). Briefly, the ORF has been PCR amplified from the pCS4+_Mermaid plasmid as follows: 0.5 µl of Pfu Ultra HQ DNA polymerase and 7.5 µl of the 10x buffer (600389, Agilent Technologies, Santa Clara, CA, US), 1 µl of 10 mM dNTPs, 2.5 µl of DMSO, 1 µl each of a 20 mM stock solution of the T3 Universal primer and the Mermaid Universal *Sma*I primer (5' TATCCCGGGATTCGACGGTTCAGATTTTA) in a total volume of 50 µl (the PCR has been primed for 15'' at 50°C and elongated for 4 minutes at 72°C, for a total number of 35 cycles). The specific PCR product has been gel purified and cloned into the pCMV-SC blunt vector (Strataclone, Agilent Technologies, Inc.1834, West Cedar Creek, TX, US). One positive clone (pCMV-SC_Mermaid) has been *Sma*I linearized for the subsequent insertion of the HuC promoter upstream the Mermaid ORF. The promoter has been synthesized by PCR using zebrafish genomic DNA as template and a pair of HuC specific primers (HuCprom-forw1_(SalI): 5'-GTAGTCGACCAGACTTGTCAAAAGGGTCCA and HuCprom-rev1: 5'-

TCCATTCTTGACGTACAAAGATG) spanning a 3150 bp region upstream the ATG (the PCR mix and conditions were the same as above). The specific band has been gel purified and cloned into the *Sma*I-linearized pCMV-SC_Mermaid plasmid to obtain the pHuC_Mermaid final construct (Figure 4) used for the subsequent FRET analysis.

Figure 4

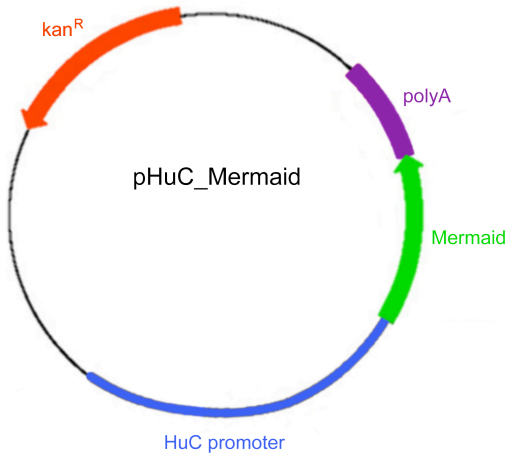

Figure 4: Schematic map of pHuC_Mermaid vector
Map of the pHuC_Mermaid vector showing the relative positions of HuC promoter followed by Mermaid open reading frame and the polyadenilation site (polyA). The vector contains kanamycin resistance (kan^R). DNA segments are not in scale.

11.2 Zebrafish embryos microinjection

One-cell fertilized eggs obtained from mSod1 and AB adult zebrafish were collected in 10 mm petri dishes, rinsed in 4°C fish water and rapidly microinjected with 200 pg of the pHuC_Mermaid DNA into the yolk using the Femtojet® microinjector (Eppendorf, Parkway, NY, US). The zygotes have been then incubated at 28°C in fish water until they reached the desired stage for the FRET analysis (Figure 5).

Figure 5

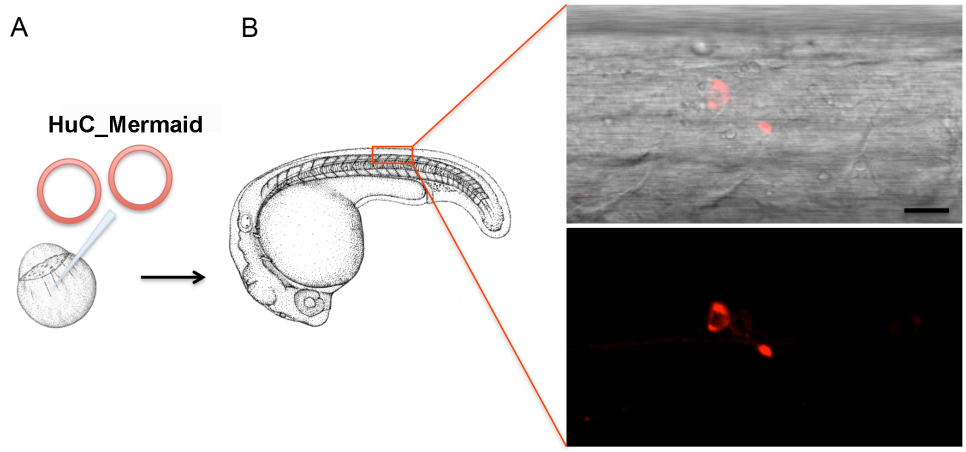

Figure 5: Mermaid is efficiently and selectively expressed in zebrafish embryonic neurons. The pHuC_Mermaid vector generated was microinjection in zebrafish embryos at one-cell stage (A). It allowed the efficient chimeric expression of the biosensor in a limited population of neurons in embryos at 20 hpf (B) as it is shown in the bright field (upper) and fluorescence (lower) images where a single motor neuron express the biosensor. Only FRET fluorescence channel is shown. Scale bar: 20 µm.

11.3 Imaging set up for Mermaid biosensor visualization in living embryos: simultaneous detection of donor and acceptor signals

Living microinjected embryos, at 20 hpf, were mounted in 1% low melting point agarose in fish water at 37°C, onto the glass of a 35 mm imaging dish with a glass bottom and gently oriented on the lateral side. When agarose solidified at RT, few drops of fish water were added and the petri dish with embryos was taken to the microscope.

Fluorescence signal was detected with the laser scanning confocal microscope Leica TCS SP5 equipped with a resonant scanner. The fluorescent proteins of FRET biosensor were contemporarily excited with the 488 nm laser line and the fluorescence emitted in the donor channel was collected setting the PMT1 bandwidth between 495 nm and 525 nm, in order to collect only mUKG signal, while the fluorescence emitted by the FRET channel (fluorescence emitted by the acceptor when the donor is excited) was simultaneously detected setting PMT2 collecting bandwidth between 550 nm and 650 nm. We acquired image fields of 512 x 64 pixels (pixel size of 605.4 nm), with 12 bits gray scale, a scan speed of 8000 Hz, without averaging and with an opened pinhole (2 airy units). Spinal neurons voltage changes in basal conditions were recorded in embryos, kept in fish water at RT, acquiring a single xy plane every 30 ms for 1 minute. The effect of riluzole on membrane depolarizations was evaluated in the same neuron after 5 minutes

from the addition of fish water containing 5 μM riluzole. In all the acquisitions, the offset was optimized at the beginning of the experimental session and set low enough so that background pixels have a measured intensity slightly greater than zero and kept constant during the entire experimental session. The gain was optimized, for each cell, to avoid saturated pixels and to maximize signal to noise ratio and was maintained the same for basal conditions and riluzole stimulation in the same cell.
At the end of the acquisition, embryos, born from mSod1 heterozygous fish intercrossing, were fixed in 4% paraformaldehyde in PBS 1x, and after DNA extraction, checked for the presence of the gene encoding for DsRed through PCR as previously described in paragraph 10. Negative embryos were considered controls (Ctrl).

11.4 Time course emission ratio calculation and voltage changes analyses

The analysis of FRET changes, during time, was performed with the ImageJ macro Biosensor_FRET (created by Robert Bagnell, Pathology & Lab Med UNC-CH, in 2010, www.med.unc.edu/microscopy/resources/imagej-plugins-and-macros/biosensor-fret): a macro able to process time-lapse image stacks made from live cells expressing single chain FRET biosensor exhibiting FRET, where it is not necessary to make bleed-through corrections, like Mermaid in our experimental settings. Briefly, with this macro we performed background subtraction in each frame of the stack choosing an appropriate background region that was used to process both the donor and the FRET stack. In that region was calculated the average intensity and it was subtracted from every pixel of every image in the stack. Then, images were masked, setting a threshold on the cells using the Image > Adjust > Threshold dialog box in a way that the background intensity is 0 (selecting “dark background”) and the cells are gray scale. The plugin subsequently started photobleaching correction by using the threshold set in the masking step. Photobleaching correction is based on the ratio of the change in mean brightness of the thresholded parts of the cells over time (Hodgson et al., 2010). FRET and donor fluorescence intensity mean values (FRET mean and Donor mean) were normalized to the first value in each set and a ratio is calculated of the normalized values. Thus ((FRET mean)^{tx}/(FRET mean)^{t1} / (Donor mean)^{tx}/(Donor mean)^{t1}) is calculated for every time point. After, the FRET / Donor raw ratio stack is calculated, each image is multiplied by the inverse of the curve value at its respective time point to correct for the amount of

photobleaching, the final FRET / Donor ratio is calculated and the photobleaching correction is applied.

In this way we obtained a curve showing normalized FRET ratio changes (y-axis) during time (x-axis) and a double exponential curve was fit to these data. We then multiplied the normalized FRET ratio calculated for each time point and the fitting curve for the effective FRET ratio calculated at t1 as ((FRET mean - FRET background)/(Donor mean - Donor background)) where FRET and Donor mean intensity is the mean fluorescence intensity calculated in the same region of interest (ROI) draw around the cell and FRET and Donor background is the mean fluorescence intensity calculated in a ROI of the field without the fluorescent sample.

For each neuron we calculated the basal membrane ratio as the mean ratio value calculated from the fitting curve and in those neurons presenting periodic depolarizations we calculated their frequency, amplitude and duration with the software GraphPad Prism® 6.0c. With this software we also statistically analyzed the data obtained with the unpaired Student t test. Means were considered statistically different when $P < 0.05$.

RESULTS

1. Sod1 OVEREXPRESSION DOES NOT AFFECT EXTERNALLY VISIBLE ANATOMY AND BODY WEIGHT OF ADULT ZEBRAFISH

We started the characterization of Sod1 overexpressing zebrafish evaluating the effects of wild-type Sod1 or mutated Sod1 expression on zebrafish anatomy at 12 months of age. Heterozygous wtSod1 and mSod1 zebrafish and AB zebrafish (Ctrl) were weighted and photographed to measure and compare the typical traits of post-embryonic zebrafish anatomy (Parichy et al., 2009): the standard length (SL), the length between the operculum and the caudal peduncle (LOCP) and the height at anterior of anal fin (HAA) (Figure 1,A). We did not observe any macroscopic alteration among zebrafish of the three genotypes, except for the bright red eyes of mSod1 zebrafish, presumably due to the high expression levels of the reporter gene DsRed in that tissue (Figure 1,B). We did not measure any significant alteration either in the standard length, or in the height at anterior of anal fin, or in the length from the operculum to the caudal peduncle or in the body weight among adult zebrafish of the three genotypes (see histograms in Figure 1,C). The numerical values are reported in Table 1.

Table 1

Anatomical Parameter	Ctrl	wtSod1	mSod1	P value summary
SL (cm)	3.03 ± 0.09 (7)	2.82 ± 0.07 (6)	2.84 ± 0.16 (7)	P = 0.310
LOCP (cm)	2.35 ± 0.08 (7)	2.17 ± 0.05 (6)	2.16 ± 0.13 (7)	P = 0.316
HAA (cm)	0.64 ± 0.03 (7)	0.56 ± 0.04 (6)	0.55 ± 0.03 (7)	P = 0.174
Body Weight (g)	0.45 ± 0.04 (15)	0.39 ± 0.03 (14)	0.46 ± 0.04 (14)	P = 0.347

Table 1. Means of the standard length (SL), of the length between the operculum and the caudal peduncle (LOCP) and of the height at anterior of anal fin (HAA), in cm, and of the body weight, in g, measured in Ctrl, wtSod1 and mSod twelve months old zebrafish.
Results were statistically analyzed with the software GraphPad Prism® 6.0c version, with One-way Analysis of Variance (ANOVA), Kruskal-Wallis test, and corrected with Dunn's multiple comparison test. Means were considered statistically different when P < 0.05.
Values are reported as mean ± SEM; the number of analyzed animals is reported in brackets. The P values obtained in the statistical analyses are shown.

2. THE EXPRESSION OF Sod1 G93R IMPAIRS ADULT ZEBRAFISH SPONTANEOUS SWIMMING ACTIVITY

In patients and rodent models of ALS, clinical abnormalities associated to weakness and muscular atrophy, appear in adulthood. Therefore, we searched for signs of motor impairments associated to the disease progression in adult zebrafish studying the spontaneous locomotor activity in twelve months old heterozygous wtSod1 and mSod1 zebrafish and AB zebrafish (Ctrl). For this study, each fish was individually put in a breeding tank, filled with sufficient fish water to guarantee an unrestrained swimming of the animal but at the same time preventing vertical movements. Three adult fish, one for each genotype, were recorded contemporarily for 10 minutes.

The analyses of the tracks swum by zebrafish during the spontaneous locomotor activity monitoring (three representative examples, one for each genotype, are displayed in Figure 2,A) revealed a significant reduction in the distance travelled and in the time spent at resting by mSod1 zebrafish compared to Ctrl fish but no differences in the swimming speed among fish of the three genotypes (graphs in Figure 2,B and Table 2).

Table 2

Swimming Activity Parameters	Ctrl	wtSod1	mSod1	P value summary
Distance Travelled (cm)	3080 ± 232	2673 ± 248	2389 ± 122	P = 0.026
Time at Resting (s)	17.73 ± 2.02	20.58 ± 1.59	28.73 ± 3.77	P = 0.014
Speed (cm/s)	6.19 ± 0.38	5.52 ± 0.25	5.77 ± 0.31	P = 0.330

Table 2. Measures of the distance travelled (cm) of the time at resting (s) and of the speed (cm/s) calculated with the MTrack2 ImageJ plugin for 15 zebrafish for each genotype. Values are reported as mean ± SEM and were collected in 4 independent experiments performed with adult zebrafish belonging to 2 different generations. The P values of the statistical analyses are reported.

All parameters were analyzed with the software GraphPad Prism® 6.0c and means were considered statistically different when $P < 0.05$. The measures of the distance travelled and of the speed were statistically analyzed with One-way Analysis of Variance (ANOVA) and corrected with Tuckey's post-test. We evaluated a significant reduction in the distance travelled by mSod1 zebrafish compared to Ctrl ($P = 0.020$) but not from

wtSod1 zebrafish (P = 0.487). There are no differences in the distance travelled between Ctrl and wtSod1 zebrafish (P = 0.234). We did not evidence any significant alteration in the speed between animals of the three genotypes (P value summary 0.330).

The values of the time at resting were statistically analyzed with One-way Analysis of Variance (ANOVA), Kruskal-Wallis test, and corrected with Dunn's multiple comparison procedure. We observed a significant increase in the time spent at resting by mSod1 zebrafish compared to Ctrl (P = 0.014) but not from wtSod1 zebrafish (P = 0.085). There are no differences in this parameter between Ctrl and wtSod1 zebrafish (P = 0.726).

3. ADULT mSod1 ZEBRAFISH SHOW A SIGNIFICANT REDUCTION IN SPINAL CORD AREA, IN MOTOR NEURONS NUMBER AND IN WHITE MUSCLE FIBERS CALIBER

To precisely characterize the phenotype associated to wtSod1 and mSod1 overexpression in the spinal cord and in the lateral muscle of adult zebrafish we performed histological analyses. Since the typical traits of adult zebrafish anatomy (SL, LOCP and HAA) do not change in twelve months old zebrafish of the three genotypes we investigated the presence of the typical hallmarks of the disease in comparable portion of the fish trunk cutting each animal in 5 segments using fins as standard anatomical references. Segment 1 (S1) results from a cut in correspondence of the operculum, segment 2 (S2) goes from the operculum to the beginning of the pelvic fin, segment 3 (S3) spans the pelvic fin till the beginning of the anal fin, segment 4 (S4) ranges from the beginning to the end of the anal fin and segment 5 (S5) extends from the end of the anal fin to the caudal peduncle (Figure 3,A). We decided to focus our attention to the spinal cord, so we did not analyze the first segment obtained containing the brain. Since all the segments produced from the zebrafish trunk were embedded with a cranial to caudal orientation, we collected and stained, with hematoxylin and eosin, histological sections from the cranial portion of all the segments under investigation. In each section, we measured the area of the spinal cord and counted the number of motor neurons, recognized thanks to their peculiar morphology (Figure 3,B). Results were statistically analyzed with the software GraphPad Prism® 6.0c version and means were considered statistically different when $P < 0.05$.

We observed a significant reduction in the area of the spinal cord (Figure 3,B and Table 3) and in the number of motor neurons (Figure 3,B and Table 4) along the entire

mSod1 zebrafish trunk in comparison to Ctrl and wtSod1 zebrafish. Ordinary Two-way Analysis of Variance (ANOVA) and Bonferroni's multiple comparisons test allowed us to assess the effect of the zebrafish genotype and of the spinal cord segment to the measure variability. Subsequently, we statistically compared data obtained in mSod1 fish with those obtained in Ctrl and wtSod1 respectively, and those obtained in wtSod1 with those gathered in Ctrl fish with ordinary Two-way Analysis of Variance (ANOVA) and Sidak's multiple comparison test.

The statistical analyses evidenced a significant effect of the segment under consideration on the area of the spinal cord ($P < 0.0001$), in fact, it gradually decreases from the rostral to the caudal portion of the zebrafish trunk, similarly, in all animals; moreover, it highlighted a significant contribution of the zebrafish genotype ($P < 0.0001$) on the mean area of the spinal cord along the entire trunk of the animal. Particularly, mSod1 fish showed a significant reduction in spinal cord area along the entire trunk compared to both Ctrl ($P < 0.0010$) and wtSod1 ($P = 0.0010$) zebrafish while there are no differences in the same parameter between Ctrl and wtSod1 ($P = 0.3465$).

Table 3

Spinal Cord Area (μm^2)	Ctrl	wtSod1	mSod1
S2	0.125 ± 0.012	0.124 ± 0.014	0.083 ± 0.002
S3	0.081 ± 0.006	0.072 ± 0.007	0.064 ± 0.007
S4	0.061 ± 0.006	0.049 ± 0.006	0.041 ± 0.003
S5	0.038 ± 0.003	0.038 ± 0.005	0.025 ± 0.006

Table 3: Spinal cord area (expressed as mean ± SEM) measured in each segment of the trunk in 7 Ctrl, 6 wtSod1 and 7 mSod1 zebrafish at 12 months of age. Data were collected in 4 independent experiments and obtained from adult zebrafish belonging to 2 different generations.

The same statistical analyses pointed out to a significant contribution of the segment under consideration to the variability of the mean number of motor neurons in each segment of the spinal cord ($P < 0.0001$). Also in this case, in fact, we observed a progressive reduction in the number of motor neurons from rostral toward caudal segments of the spinal cord. This trend is similar in animals of each genotype examined. We assessed also a significant contribution of the zebrafish genotype ($P = 0.0040$) on the mean number of motor neurons along the entire spinal cord; in fact, mSod1 fish exhibited

a significant reduction in motor neurons number along the entire spinal cord compared to both Ctrl ($P < 0.0014$) and wtSod1 ($P = 0.0057$) zebrafish, while there are no differences in the same parameter between Ctrl and wtSod1 ($P = 0.8582$).

Table 4

Motor neurons (n)	Ctrl	wtSod1	mSod1
S2	17.75 ± 1.41	15.97 ± 1.71	12.11 ± 1.35
S3	12.93 ± 1.28	12.04 ± 2.46	10.11 ± 1.47
S4	10.79 ± 0.91	11.33 ± 2.57	7.86 ± 1.22
S5	9.00 ± 3.04	10.17 ± 1.17	5.29 ± 1.57

Table 4: Motor neurons number (reported as mean ± SEM) counted in the indicated segment of the trunk in 7 Ctrl, 6 wtSod1 and 7 mSod1 zebrafish. Values were collected in 4 independent experiments with adult fish belonging to 2 different generations.

Since one of the main features of ALS is muscular atrophy we searched for alterations in muscle fibers in the same segments of the body wall. We focused our attention on white muscle fibers because they represent the most relevant component of zebrafish musculature and of the entire body wall (Figure 3,C). Red fibers constitute a very thin layer of fibers immediately under the skin that are inhomogenously present in the different segments under investigation and that are often lost while cutting paraffin sections, thus preventing an accurate examination. We measured white muscle fibers caliber as Feret diameter (the longest distance between any two points along the polygonal ROI drawn around each fiber) in at least 100 hundred fibers in each body segment. We used ordinary Two-way Analysis of Variance (ANOVA) and Bonferroni's multiple comparisons test to assess the effect of the zebrafish genotype and of the trunk segment to the measure variability. Subsequently we statistically compared mean fiber caliber obtained in mSod1 fish with that obtained in Ctrl and wtSod1 fish, and that obtained in wtSod1 with those gathered in Ctrl zebrafish with ordinary Two-way Analysis of Variance (ANOVA) and Sidak's multiple comparison test. In all cases, means were considered statistically different when $P < 0.05$.

We observed a significant reduction in the mean white fibers caliber in mSod1 zebrafish compared to Ctrl fish, along the entire trunk, particularly severe in the most caudal portion of the body wall (Figure 3,C and Table 5).

Table 5

White Fibers Caliber (µm)	Ctrl	wtSod1	mSod1
S2	69.46 ± 2.56	68.76 ± 4.71	62.53 ± 5.37
S3	70.13 ± 3.12	67.26 ± 3.50	64.71 ± 5.40
S4	70.56 ± 1.75	64.06 ± 3.48	54.95 ± 4.80
S5	65.59 ± 2.81	58.65 ± 5.46	51.92 ± 6.07

Table 5: White muscle fibers caliber (reported as mean ± SEM) measured in the indicated trunk segment in 6 Ctrl, 6 wtSod1 and 6 mSod1 zebrafish. Data were collected in 4 independent experiments with adult zebrafish belonging to 2 different generations.

This time, the statistical analyses did not highlight a variation of white fiber caliber in the different segments of zebrafish trunk ($P = 0.0883$). However, we observed a significant variability of the white fiber caliber along the entire spinal cord among zebrafish of the three genotypes ($P = 0.0298$). mSod1 zebrafish presented a significant reduction in white fibers caliber along the trunk compared to Ctrl ($P = 0.0013$) fish, particularly severe in the most caudal segments of the trunk (S4-S5), while there are no differences compared to wtSod1 ($P = 0.0849$). White fibers caliber did not significantly change between Ctrl and wtSod1 zebrafish ($P = 0.1025$).

We examined the ultrastructure of adult white muscle fibers of zebrafish trunk with the electron microscope. Particularly, we focused our attention to the fine structural organization of sarcomeres and performed the morphometric analyses of muscular mitochondria measuring their area, perimeter and circularity in Ctrl and mSod1 zebrafish. We did not observed any alteration in the organization of the contractile apparatus but, preliminary results obtained analyzing more than 100 mitochondria in one animal per genotype evidenced a significant reduction in the area, perimeter and circularity of muscular mitochondria in mSod1 zebrafish compared to Ctrl zebrafish (Table 6) without other defects in mitochondria ultrastructure (cristae disorganization or swelling).
Data were statistically analyzed with the software GraphPad Prism® 6.0c version, with Student t test, and means were considered statistically different when $P < 0.05$.

Table 6

Ultrastructural Analyses	Ctrl	mSod1	P value
M - Area (μm^2)	0.98 ± 0.06	0.68 ± 0.03	P < 0.0001
M - Perimeter (μm)	3.48 ± 0.98	3.02 ± 0.08	P < 0.0001
M - Circularity (c.i.)	0.95 ± 0.02	0.90 ± 0.01	P < 0.0001

Table 6: Mitochondrial (M) area (μm2) perimeter (μm) and circularity (c.i.) of muscular mitochondria measured in electron micrographs of 12 months old Ctrl and mSod1 muscles. Values are reported as mean ± SEM. P values obtained in the statistical analyses are reported

4. WHITE LATERAL MUSCLE OF mSod1 ZEBRAFISH IS SIGNIFICANTLY DENERVATED

The degree of innervation was studied on cryostat sections of lateral white muscles of zebrafish trunk at one year of age. We performed fluorescence staining against SV2A and AChRs (Figure 4,A) and we evaluated the percentage of innervation as the percentage of postsynaptic acetylcholine receptors clusters facing synaptic vesicles presynaptic clusters. We further investigated the density and the dimensions of pre and postsynaptic elements and the fluorescence intensity associated.

We measured a significant reduction in the percentage of innervation of white lateral muscles of mSod1 zebrafish compared to Ctrl fish (Figure 4,B and Table 7); a significant reduction in the density of presynaptic structures but not in that of postsynaptic one (Figure 4,B and Table 7) without any changes in pre and post synaptic clusters size (Figure 4,B and Table 7) and in the fluorescence intensity signal associated (Figure 4,B and Table 7).

Despite the extent of denervation, the ultrastructural analyses of adult zebrafish neuromuscular junctions revealed that residual presynaptic boutons in the white lateral muscle of mSod1 zebrafish did not show peculiar morphological alterations (data not shown).

Table 7

	Ctrl	mSod1	P value
Innervation (%)	95.94±0.84	57.48±8.69	0.0043
Presynaptic clusters density (clusters /µm^2) x 10^{-4}	8.69 ± 0.06	5.76 ± 0.09	0.0303
Postsynaptic clusters density (clusters /µm^2) x 10^{-4}	9.04 ± 0.06	9.96 ± 0.05	0.3290
Presynaptic clusters size (µm^2)	0.54±0.05	0.48±0.03	0.3971
Postsynaptic clusters size (µm^2)	2.36±0.33	1.89±0.26	0.2994
Presynaptic clusters fluorescence intensity (a.u.)	25.56±1.39	28.34±2.42	0.3488
Postsynaptic clusters fluorescence intensity (a.u.)	16.09±3.16	14.88±2.16	0.7616

Table 7: Innervation percentage (%), pre and postsynaptic clusters density (clusters/µm^2), pre and post synaptic clusters size (µm^2) and their fluorescence intensity signal (a.u.) measured in the white lateral muscles of 5 Ctrl and 6 mSod1 zebrafish. Values are reported as mean ± SEM and were collected in 2 independent experiments performed with adult zebrafish belonging to 2 different generations. Results were statistically analyzed with the Student t test and P values obtained are reported. Means were considered statistically different when P < 0.05.

5. TRANSGENIC ZEBRAFISH EXPRESSING Sod1 PRESENT REACTIVE ASTROGLIOSIS IN THE SPINAL CORD AND ACTIVATED INFLAMMATORY CELLS INFILTRATE mSod1 LATERAL MUSCLES

Although the molecular mechanism underlying motor neurons degeneration remains unknown, non-neuronal cells (including astrocytes and microglial cells) shape motor neuron survival in ALS.

Astrocytes closely interact with neurons to provide an optimized environment for neuronal function and respond to all forms of injury in a typical manner known as reactive astrogliosis. A strong reactive astrogliosis surrounds degenerating motor neurons in ALS patients and ALS-animal models.

Microglia, derived from the hematopoietic cell lineage, are generally considered as the primary immune cells of the central nervous system. They sense and react to many types of damage including those produced in neurodegenerative diseases. Extensive microgliosis and inflammation have been reported in mutant SOD1 transgenic mice.

Since reactive astrogliosis and microgliosis are considered specific hallmarks of the disease in patients and rodent models of ALS, we performed immunofluorescence

experiments on histological sections either with antibodies against Gfap (an astrocytes marker) or Aif1 (a marker for activated microglia in the spinal cord and activated macrophages and neutrophils at the periphery) in the attempt to evaluate if the zebrafish model expressing mSod1 present this phenotype.

We acquired Gfap and Aif1 fluorescence signal in zebrafish spinal cord in S2-S5 segments of 7 Ctrl, 6 wtSod1 and 7 mSod1 zebrafish at 12 months of age (Figure 5,A) and we compared the ratio between the mean fluorescence intensity measured in the spinal cord and the area of the spinal cord itself (Figure 5,A and Table 8 and 9). Results were statistically analyzed with the software GraphPad Prism® 6.0c version, with ordinary Two-way Analysis of Variance (ANOVA) and Bonferroni's multiple comparisons test to verify the effect of the zebrafish genotype and of the spinal cord segment to the measure variability. Subsequently we statistically compared Gfap or Aif1 mean fluorescence intensity per spinal cord μm^2 in mSod1 fish with that obtained in Ctrl and wtSod1 fish, and that obtained in wtSod1 with those measured in Ctrl zebrafish with ordinary Two-way Analysis of Variance (ANOVA) and Sidak's multiple comparison tests. In all cases, means were considered statistically different when $P < 0.05$.

Statistical analyses revealed a significant ($P < 0.0001$) contribution of spinal cord segment under investigation to the variability of Gfap and Aif1 fluorescence intensity per spinal cord μm^2, in fact, there is a progressive increase of the fluorescence signal toward the most caudal segment of the trunk in all animals. However, the increase in Gfap (Table 8) fluorescent signal per spinal cord μm^2 along the spinal cord is significantly different among zebrafish of the three genotypes ($P = 0.0246$); in particular, it is significantly higher both in wtSod1 ($P = 0.0117$) and in mSod1 ($P = 0.0177$) zebrafish compared to Ctrl zebrafish. This increase, in mSod1 zebrafish, is particularly pronounced in the last segment of the spinal cord.

Concerning Aif1 fluorescence signal per spinal cord μm^2, despite a progressive increase of the signal toward the caudal segments of the spinal cord, there are no significant differences in the signal measured among zebrafish of the three genotypes ($P = 0.1413$) (Table 9).

Table 8

Gfap (a.u./μm^2)x10^{-3}	Ctrl	wtSod1	mSod1
S2	0.14 ± 0.03	0.14 ± 0.03	0.24 ± 0.06
S3	0.24 ± 0.05	0.22 ± 0.04	0.28 ± 0.07
S4	0.33 ± 0.05	0.45 ± 0.07	0.46 ± 0.07
S5	0.49 ± 0.05	0.71 ± 0.03	0.69 ± 0.11

Table 8: Gfap fluorescence intensity in arbitrary units (a.u.) per spinal cord area in μm^2 measured in 7 Ctrl, 6 wtSod1 and 7 mSod1 zebrafish. Values are reported as mean ± SEM and were collected in 2 independent experiments performed with adult zebrafish belonging to 2 different generations. Results were statistically analyzed with the Two-way Analysis of Variance (ANOVA).

Table 9

Aif1 (a.u./μm^2)x10^{-3}	Ctrl	wtSod1	mSod1
S2	0.17 ± 0.03	0.16 ± 0.02	0.20 ± 0.04
S3	0.25 ± 0.05	0.21 ± 0.03	0.27 ± 0.06
S4	0.34 ± 0.03	0.44 ± 0.01	0.41 ± 0.07
S5	0.54 ± 0.10	0.81 ± 0.05	0.70 ± 0.14

Table 9: Aif1 fluorescence intensity in arbitrary units (a.u.) per spinal cord area in *μm^2 measured in 7 Ctrl, 6 wtSod1 and 7 mSod1 zebrafish. Values are reported as mean ± SEM and were collected in 2 independent experiments performed with adult zebrafish belonging to 2 different generations. Results were statistically analyzed with the Two-way Analysis of Variance (ANOVA).*

Since Aif1 is a marker for activated macrophages and neutrophils in the peripheral tissues we analyzed also the presence of activated inflammatory cells in the lateral muscle of the zebrafish trunk (Figure 5,B). We measured the mean number of Aif1 positive cells per μm^2 of muscle and the percentage of the area occupied by Aif1 fluorescent signal in white lateral muscle of adult zebrafish. Results were statistically analyzed with ordinary Two-way Analysis of Variance (ANOVA) and Bonferroni's multiple comparisons test to verify the effect of the zebrafish genotype and of the spinal cord segment to the measure variability. Subsequently, we statistically compared the mean number of Aif1 positive cells and the mean percentage of Aif1 fluorescence area in mSod1 zebrafish with that obtained in Ctrl and wtSod1 fish, and that obtained in wtSod1 with those measured in Ctrl zebrafish with ordinary Two-way Analysis of Variance (ANOVA) and Sidak's multiple comparison tests. Means were considered statistically different when $P < 0.05$.

Both in the case of the number of Aif1 positive cells and in the percentage of Aif1 fluorescence signal in the zebrafish lateral muscle, no significant differences can be detected in the parameter calculated among the different trunk segments of the animal under investigation (P = 0.1111 and P = 0.5641, respectively). However, in both cases, the mean values of the two parameters calculated in the animals of the three genotypes are significantly different (P < 0.0001 in both cases).

In fact, in mSod1 zebrafish there is an extremely significant increase both in the number of Aif1 positive cells compared to Ctrl (P < 0.0001) and wtSod1 fish (P = 0.0177) (Figure 5,B and Table 10) and in the percentage of Aif1 positive area compared to Ctrl (P < 0.0003) and wtSod1 (P = 0.0002) animals (Figure 5,B and Table 11) in all trunk segments.

Table 10

Aif1 positive cells (cells/μm^2) x10^{-3}	**Ctrl**	**wtSod1**	**mSod1**
S2	0.19 ± 0.11	0.05 ± 0.04	0.92 ± 0.28
S3	0.26 ± 0.02	0.21 ± 0.14	1.77 ± 0.06
S4	0.36 ± 0.03	0.19 ± 0.10	1.67 ± 0.41
S5	0.24 ± 0.01	0.04 ± 0.03	1.43 ± 0.42

Table 10: Density of Aif1 positive cells in the white lateral muscle of zebrafish at 12 months of age measured in 3 Ctrl, wtSod1 mSod1 zebrafish. Values are reported as mean ± SEM. Results were statistically analyzed with the Two-way Analysis of Variance (ANOVA).

Table 11

Aif1 positive area (%)	**Ctrl**	**wtSod1**	**mSod1**
S2	0.079 ± 0.060	0.011 ± 0.009	0.786 ± 0.335
S3	0.068 ± 0.020	0.073 ± 0.006	1.318 ± 0.194
S4	0.136 ± 0.017	0.085 ± 0.057	1.576 ± 0.736
S5	0.088 ± 0.069	0.015 ± 0.012	1.059 ± 0.444

Table 11: Percentage of the area occupied by Aif1 fluorescence signal in white lateral muscles of 3 Ctrl, wtSod1 and mSod1 zebrafish. Values are reported as mean ± SEM. Results were statistically analyzed with the Two-way Analysis of Variance (ANOVA).

6. THE EXPRESSION OF COMPLEX MOTOR BEHAVIORS IS ASSOCIATED WITH MORPHOLOGICAL AND ULTRASTRUCTURAL CHANGES OF THE DEVELOPING LOCOMOTOR NETWORK

Since adult zebrafish expressing the mutated form of Sod1 present the major hallmarks of ALS and are revealing promising models for the study of the pathology we decided to characterize the morphological features of the developing zebrafish locomotor network in search of precocious alterations that could be associated to the pathology.
We morphologically compared the developing locomotor network of Ctrl, wtSod1 and mSod1 zebrafish at three stages of development characterized by the expression of peculiar motor responses. We studied embryos 20 hpf when they undergo a transient period of alternating tail coilings and 48 hpf when they respond to touch with fast coilings of the trunk and finally we studied larvae 96 hpf when they start expressing an organized swimming (Figure 6,A).

Whole mount immunofluorescence staining reveals that 24 hpf Ctrl embryos show short motor axons, protruding from the spinal cord, filled with synaptic vesicles (green) travelling along the entire axonal length. Motor axons outgrowth follows a rostral to caudal developmental wave and only more rostral motor nerves present branches. Acetylated tubulin (gray) stains few spinal interneurons axonal projections and at this developmental stage, we do not detect AChRs clusters along muscular fibers precursors plasmamembrane. The ultrastructural analysis shows axonal projections, filled with synaptic vesicles, with immature boutons facing muscular fibers precursor presenting a cytoplasm filled with glycogen and where the contractile apparatus is poorly organized (Figure 6,B).

Forty-eight hpf embryos show motor nerves presenting a well organized microtubule network along their entire length. Spinal motor axons deeply protrude in the trunk along myosepta and they start innervating muscular fiber precursors with several branches. Synaptic vesicles do not follow the entire axonal length but are well organized in small clusters at the tips of axonal branches. AChRs start organizing in visible clusters on muscular fibers, independently from presynaptic terminals maturation (Panzer et al., 2005); in fact, most of them are not associated to a presynaptic element. Electron micrographs show presynaptic terminals filled with vesicles mainly located at the periphery of myotomes while muscle fiber precursors now display a well organized contractile apparatus (Figure 6,C).

Zebrafish larvae 96 hpf show well developed motor nerves, heavily branched, innervating muscle fibers. Synaptic vesicles are distributed in smaller clusters at the tips of axonal terminals and now face AChRs clusters on muscle fibers. The ultrastructural analysis shows small presynaptic boutons, deeply penetrating inside the myotomes, and innervating well developed muscle fibers. Zebrafish muscle fibers do not develop peculiar postsynaptic specializations (Figure 6,D).

Our observations confirm that the progressive capabilities to perform complex motor responses during zebrafish development are associated to the progressive morphological maturation of the locomotor network.

As a result of these examinations, we decided to investigate whether the expression of wild-type or mutant Sod1 affects: 1) motor axons morphology 24 and 48 hpf 2) motor behaviors in embryos and larvae 20, 48 and 96 hpf; 3) pre and postsynaptic clusters maturation and assembly in mature neuromuscular synapses 48 and 96 hpf with a detailed ultrastructural analysis of presynaptic terminals and muscle fibers at this latter stage of development.

7. Sod1 EXPRESSION CAUSES SPINAL MOTOR AXONS MORPHOLOGICAL ALTERATIONS AT 24 hpf

We started the characterization of Sod1 overexpressing zebrafish developing motor nerves at 24 hpf. To this aim, we performed whole mount fluorescence staining experiments against SV2A, AChRs and acetylated tubulin in 24 hpf Ctrl, wtSod1 and mSod1 embryos. Since, at this stage of development, synaptic vesicles travel along the entire motor axons length (Figure 6,B); we measured motor axons length, unbranched axonal length (as the axonal length ranging from the axonal emerging site from the spinal cord to the first axonal branching point) and number of axonal branches, in at least 5 motor nerves for each animal, in confocal fluorescence maximum projection images of SV2A signal in the region ranging from the 12^{th} and the 16^{th} somite (Figure 7,A and Table 12) and in the region ranging from the 17^{th} and the 21^{st} somite (data not shown).
Results were statistically analyzed with One-way Analysis of Variance (ANOVA) or Kruskal-Wallis test and corrected with Tuckey's or Dunn's multiple comparison test. Means were considered statistically different when $P < 0.05$

We measured a significant reduction in the motor axons length in wtSod1 ($P = 0.0006$) and mSod1 ($P < 0.0001$) embryos compared to Ctrl fish, we detected a significant

reduction in the unbranched axonal length in wtSod1 ($P = 0.0208$) and mSod1 ($P < 0.0001$) compared to Ctrl embryos and we evidenced a significant increase in the number of axonal branches in mSod1 embryos compared to both Ctrl ($P < 0.0001$) and wtSod1 embryos ($P = 0.0469$) (Figure 7,B). In this case, we did not detect significant differences in the number of axonal branches between Ctrl and mSod1 embryos.

Table 12

Morphological Parameter	Ctrl	wtSod1	mSod1
Motor Axons Length (μm)	95.6 ± 2.4	78.9 ± 2.8	73.1 ± 3.5
Unbranched Axonal Length (μm)	73.0 ± 2.8	55.0 ± 3.5	38.0 ± 4.3
Number of branches (n)	1.9 ± 0.2	2.4 ± 0.3	3.8 ± 0.4

Table 12: Motor axons length (μm), unbranched axonal length (μm) and number of branches (n) measured in 25 Ctrl, 17 wtSod1 and 21 mSod1 PCR genotyped embryos (see Materials and Methods) in correspondence of the 12th and the 16th somite. Values are reported as mean ± SEM and were collected in 3 or 4 independent experiments.

Similar results were obtained analyzing the morphology of spinal motor nerves between the 17th and the 21st somite (data not shown).

8. Sod1 EXPRESSING EMBRYOS DO NOT SHOW ALTERATIONS IN MOTOR NERVES MORPHOLOGY AT 48 hpf BUT, THOSE EXPRESSING G93R Sod1, PRESENT DEFECTS IN SYNAPTIC VESICLES CLUSTERIZATION

We compared the morphology of the locomotor network, after whole mount fluorescence staining experiments for SV2A, AChRs and acetylated tubulin, in Ctrl, wtSod1 and mSod1 embryos at 48 hpf.

Since at this developmental stage, synaptic vesicles do not depict the entire axonal length (Figure 6,C) we measured motor axons length, unbranched axonal length and number of axonal branches, in at least 4 motor nerves for each animal, in confocal fluorescence maximum projection images of acetylated tubulin signal in the region ranging from the 9th and the 13th somite (Figure 8,A).

We did not measure any significant difference both in motor axons length, unbranched axonal length and number of branches in Ctrl, wtSod1 and mSod1 embryos (Figure 8,B and Table 13).

Table 13

Morphological Parameter	Ctrl	wtSod1	mSod1	P value
Motor Axons Length (μm)	147.2 ± 5.2	139.3 ± 4.6	135.1 ± 5.5	0.5895
Unbranched Axonal Length (μm)	28.9 ± 4.8	6.6 ± 2.1	7.9 ± 2.2	0.3338
Number of branches (n)	18.1 ± 2.5	19.7 ± 2.1	22.1 ± 1.8	0.3953

Table 13: Motor axons length (μm), unbranched axonal length (μm) and number of branches (n) measured in correspondence of the 9th - 13th somites in 10 Ctrl, 10 wtSod1 and 13 mSod1 48 hpf embryos screened thanks to DsRed expression after heat shock at 24 hpf (see Materials and Methods). Values are reported as mean ± SEM and were collected in 2 or 3 independent experiments. Data were statistically analyzed with One-way Analysis of Variance (ANOVA) and corrected with Tuckey's post-test. Means were considered statistically different when P < 0.05. P values obtained are reported.

Since at this stage of development, synaptic vesicles start clustering at the tips of motor nerves branches and AChRs organizes in visible clusters on muscular precursors plasmamembrane, thanks to the ImageJ Plugin JACoP we performed a 3D object-based colocalization analysis to evaluate the density of total pre and post synaptic clusters and of pre and postsynaptic colocalizing clusters in the muscles of the same portion of the trunk. We did not identify any differences in the density of both total and colocalizing pre (Figure 8,C and Table 14) and postsynaptic clusters (Figure 8,E and Table 14) at this stage of development. We also analyzed synaptic vesicles and AChRs cluster size and we assessed a significant increase in vesicles clusters size in mSod1 embryos compared to both Ctrl (P = 0.0387) and mSod1 (P = 0.0232) embryos without any significant changes in the size of AChRs clusters (Figure 8,D and Table 14).

Table 14

	Ctrl	wtSod1	mSod1	P value
Presynaptic clusters (clusters/μm^2) x10^{-4}	3.39 ± 0.74	2.99 ± 0.40	3.11 ± 0.40	0.9821
Colocalizing presynaptic clusters (clusters/μm^2) x10^{-4}	0.62 ± 0.18	0.86 ± 0.24	0.74 ± 0.19	0.7421
Postsynaptic clusters (clusters/μm^2) x10^{-4}	3.20 ± 0.80	3.88 ± 0.49	2.50 ± 0.39	0.1637
Colocalizing postsynaptic clusters (clusters/μm^2) x10^{-4}	0.56 ± 0.15	0.72 ± 0.19	0.69 ± 0.18	0.8071
Presynaptic clusters size (μm^2)	2.64 ± 0.43	2.48 ± 0.39	4.02 ± 0.39	0.0093
Postsynaptic clusters size (μm^2)	0.94 ± 0.16	1.68 ± 0.44	1.48 ± 0.29	0.1709

Table 14: Pre and postsynaptic clusters density (clusters/μm2), pre and postsynaptic colocalizing clusters density (clusters/μm2) and pre and post synaptic clusters size (μm2) measured in the muscle of 10 Ctrl, 9 wtSod1 and 13 mSod1 zebrafish screened thanks to DsRed expression after heat shock at 24 hpf (see Materials and Methods). Values are reported as mean ± SEM and were collected in 2 or 3 independent experiments. Data were statistically analyzed with One-way analysis of Variance (ANOVA) or Kruskal-Wallis test and corrected with Tuckey's or Dunn's post-test. Means were considered statistically different when P < 0.05. P values obtained in statistical analyses are reported.

9. mSod1 LARVAE EXHIBIT A SEVERE IMPAIRMENT IN NEUROMUSCULAR JUNCTIONS MATURATION AT 96 hpf

We could not analyze motor nerves morphology in zebrafish larvae at 96 hpf because of the extremely complex axonal arborization at this developmental stage, but we could follow the maturation of neuromuscular junctions (Figure 6,D and Figure 9,A) performing a 3D colocalization analysis of pre and postsynaptic clusters and measuring their dimensions as it was described at 48 hpf.

At this developmental stage, we did not observe any significant differences in synaptic vesicles and AChRs clusters size in larvae of the three genotypes (Figure 9,B and Table 15) but we evidenced a significant reduction in the density of presynaptic clusters in mSod1 larvae compared to both Ctrl (P = 0.0359) and wtSod1 (P = 0.0379) larvae. Moreover, although the density of AChRs clusters is similar among larvae of the three genotypes, we identified a significant reduction both in presynaptic colocalizing clusters in mSod1 compared to both Ctrl (P = 0.0003) and wtSod1 (P = 0.0002) larvae

and in the density of postsynaptic colocalizing clusters in mSod1 larvae in comparison to both Ctrl (P = 0.0004) and wtSod1 (P = 0.0002) larvae (Figure 9,B and Table 15).

Table 15

	Ctrl	wtSod1	mSod1	P value
Presynaptic clusters (clusters/μm^2) x10^{-3}	1.25 ± 0.02	1.26 ± 0.01	0.84 ± 0.01	0.0145
Colocalizing presynaptic clusters (clusters/μm^2) x10^{-3}	0.46 ± 0.01	0.59 ± 0.11	0.19 ± 0.01	< 0.0001
Postsynaptic clusters (clusters/μm^2) x10^{-3}	0.79 ± 0.01	0.86 ± 0.11	0.84 ± 0.01	0.3068
Colocalizing postsynaptic clusters (clusters/μm^2) x10^{-3}	0.45 ± 0.01	0.58 ± 0.01	0.19 ± 0.01	< 0.0001
Presynaptic clusters size (μm^2)	6.46 ± 0.34	7.33 ± 0.39	6.24 ± 0.43	0.1195
Postsynaptic clusters size (μm^2)	5.15 ± 0.22	6.09 ± 0.28	5.09 ± 0.49	0.0600

Table 15: Pre and postsynaptic clusters density (clusters/μm^2), pre and postsynaptic colocalizing clusters density (clusters/μm^2) and pre and post synaptic clusters size (μm^2) measured in the muscle of 19 Ctrl, 12 wtSod1 and 16 mSod1 zebrafish screened thanks to DsRed expression after heat shock at 24 hpf (see Materials and Methods). Values are reported as mean ± SEM and were collected in 3 independent experiments. Measures were statistically analyzed with Kruskal-Wallis test and corrected with Dunn's multiple comparison procedure. Means were considered statistically different when P < 0.05. P values obtained in statistical analyses are reported.

10. NEUROMUSCULAR JUNCTIONS ULTRASTRUCTURE IS PRESERVED IN mSod1 LARVAE

To evaluate if the alterations in neuromuscular junctions (NMJs) maturation observed at the confocal microscope, in zebrafish larvae at 96 hpf, were associated to ultrastructural defects in the presynaptic terminals we analyzed the fine structure of Ctrl, wtSod1 and mSod1 neuromuscular junctions. The small presynaptic boutons of zebrafish larvae contain a lot of vesicles widely distributed in the presynaptic terminal, without a peculiar polarization, and often include mitochondria. They are separated from muscle fibers by a well-defined synaptic cleft (Figure 10,A). We measured NMJs area and we performed a morphometric analysis for both synaptic vesicles and mitochondria on electron micrographs. In particular, we evaluated area, density, perimeter and circularity for both synaptic vesicles and mitochondria (all results are reported in Table 16, some of

them are graphically shown in Figure 10,B). Morphometric analyses did not reveal any differences in the area of neuromuscular junctions, in the density and morphology of synaptic vesicles (diameter, circularity, area and perimeter) and in the number and morphology of mitochondria (diameter, circularity, area and perimeter) in the presynaptic terminals among larvae of the three genotypes (Figure 10,B and Table 16).

Table 16

	Ctrl	**wtSod1**	**mSod1**	**P value**
NMJ Area (μm^2)	0.66 ± 0.10	0.69 ± 0.07	0.59 ± 0,04	P = 0.8286
Vesicle Density (Vesicles/μm^2)	227.10 ± 53.33	182.50 ± 64.10	226.70 ± 46.38	P = 0.6286
Vesicle Area (nm^2)	588.80 ± 36.45	695.10 ± 128.90	677.40 ± 52.55	P = 0.6643
Vesicle Perimeter (nm)	87.08 ± 3.32	94.83 ± 10.28	93.46 ± 4.31	P = 0.6643
Vesicle Diameter (nm)	31.20 ± 1.07	34.42 ± 3.60	33.55 ± 1.44	P = 0.6643
Vesicle Circularity (c.i.)	0.94 ± 0.02	0.92 ± 0.02	0.93 ± 0.02	P = 0.8786
Mitochondria Number per NMJ	0.95 ± 0.15	0.90 ± 0.20	0.80 ± 0.10	P = 0.8667
Mitochondria Area (μm^2)	0.08 ± 0.01	0.12 ± 0.03	0.08 ± 0.01	P = 0.3393
Mitochondria Perimeter (µm)	1.07 ± 0.06	1.28 ± 0.14	1.11 ± 0.05	P = 0.3393
Mitochondria Diameter (µm)	0.36 ± 0.02	0.46 ± 0.04	0.43 ± 0.05	P = 0.2000
Mitochondria Circularity (c.i.)	0.85 ± 0.01	0.85 ± 0.04	0.80 ± 0.04	P = 0.6286

Table 16: Morphometric analyses of NMJs, synaptic vesicles and NMJs mitochondria performed on structures collected in 10 NMJs for each animal under investigation (3 Ctrl, 3 wtSod1 and 3 mSod1 zebrafish larvae). Values are reported as mean ± SEM. Measures were statistically analyzed with Kruskal-Wallis test and corrected with Dunn's multiple comparison procedure. Means were considered statistically different when P < 0.05. P values obtained in the statistical analyses are reported.

11. LARVAE EXPRESSING mSod1 PRESENT A SIGNIFICANT REDUCTION IN MUSCLE FIBERS CALIBER AND MITOCHONDRIAL AREA WITH A PRESERVATION OF THE SARCOMERE ULTRASTRUCTURE

In 96 hpf zebrafish larvae we investigated the morphological phenotype of muscular fibers. At this developmental stage, in fact, muscular precursors complete their differentiation and appear as individual fibers with a well-organized contractile apparatus. To this aim, we analyzed muscle fibers caliber and sarcomeres organization with Second Harmonic Generation (SHG) signal microscopy (a non-linear optical process arising from the interaction of light with highly ordered arrangements of myosin filaments in muscle fibers) and we performed the ultrastructural characterization of sarcomeres and muscular mitochondria with transmission electron microscopy (Figure 11).

We acquired z-stacks of myosin SHG signal in the trunk of 17 Ctrl, 15 wtSod1 and 18 mSod1 larvae in correspondence of the 12th and the 15th somite (Figure 11,A shows a maximum projection image of myosin SHG signal collected in this portion of the trunk in a mSod1 larva). For each animal, we measured the caliber of about 35-70 fibers in individual images of myosin SHG signal acquired at different depths inside the myotomes (Figure 11,B) and the length of 30-60 sarcomeres in several different fibers, as the distance between two minima in the myosin SHG signal intensity plot profiles obtained along the longitudinal axis of the fibers (Figure 11,C). We evidenced a significant reduction in muscle fibers caliber in mSod1 larvae compared to Ctrl (P = 0.0032) fish (Figure 11,B and Table 17) without alterations in sarcomeres length (Table 17) and their organization inside the fibers.

Table 17

Myosin SHG signal analyses	Ctrl	wtSod1	mSod1	P value
Fiber caliber (µm)	6.28 ± 0.26	5.82 ± 0.30	5.13 ± 0.16	P = 0.0043
Sarcomere Length (µm)	1.89 ± 0.03	1.85 ± 0.03	1.90 ± 0.04	P = 0.7124

Table 17: Fiber caliber (µm) and sarcomere length (µm) measured in 17 Ctrl, 15 wtSod1 and 18 mSod1 myosin SHG signal z-stacks of larvae muscles analyzed in 3 different experimental sessions. Values are reported as mean ± SEM. Statistical analysis was performed with One-way Analysis of Variance (ANOVA) and Tuckey's multiple comparison post-test. Means were considered statistically different when P < 0.05. P values obtained in the statistical analyses are reported.

Electron micrographs show the intact fine structure of sarcomeres in Ctrl, wtSod1 and mSod1 larvae at 96 hpf. The measure of the length of 100 sarcomeres in 2 larvae for each genotype further confirmed the preservation of the contractile apparatus in mutant larvae (Figure 11,D and Table 18).

We performed the morphometric analysis of muscular mitochondria measuring their area, perimeter and circularity. We detected a significant reduction in the area of muscular mitochondria but not in the perimeter and circularity in mSod1 larvae compared to wtSod1 and Ctrl larvae (Figure 11,E and Table 18). We analyzed 100 mitochondria in the muscle of 6 Ctrl, 4 wtSod1 and 6 mSod1 larvae.

Table 18

Ultrastructural Analyses	Ctrl	wtSod1	mSod1	P value
Sarcomere Length (µm)	1.65 ± 0.02	1.68 ± 0.01	1.69 ± 0.01	0.2765
M - Area (μm^2)	0.89 ± 0.09	0.82 ± 0.12	0.54 ± 0.04	0.0219
M - Perimeter (µm)	3.66 ± 0.23	3.44 ± 0.25	2.93 ± 0.19	0.0895
M - Circularity (c.i.)	0.81 ± 0.02	0.79 ± 0.03	0.79 ± 0.03	0.7604

Table 18: Sarcomere length (µm) and area (μm^2) perimeter (µm) and circularity (c.i.) of muscular mitochondria measured in electron micrographs of 6 Ctrl, 4 wtSod1 and 6 mSod1 larvae. Data were statistically analyzed with One-way Analysis of Variance (ANOVA) and corrected with Tuckey's multiple comparison test. Means were considered statistically different when $P < 0.05$. Values are reported as mean ± SEM. P values obtained in the statistical analyses are reported.

12. mSod1 EMBRYOS DISPLAY AN INCREASED FREQUENCY OF SPONTANEOUS TAIL COILINGS AT 20 hpf

Since the expression of mutant Sod1 is associated to precocious alterations in locomotor network morphology: motor axons branching defects, neuromuscular junctions development impairments and muscle fibers caliber reduction; we decided to perform behavioral test to assess if morphological abnormalities were associated to alterations in motor responses.

One of the advantages of zebrafish, as a model for the study of the locomotor network, is that, each step in the progressive refinement of locomotor circuits during development is accompanied by the appearance of transient, more and more complex, stereotyped motor responses. The stereotypic motor activity of the developing zebrafish includes three sequentially appearing behaviors (Figure 6,A): a transient period of

alternating tail coilings (between 17 and 24 hpf) followed by touch response (starting from 24 hpf) and the appearance of organized swimming (96 hpf) (Brustein et al., 2003). We studied all these behavioral responses in wtSod1 and mSod1 embryos and larvae to identify motor alterations associated to the transgene expression.

Spontaneous tail coilings are embryonic movements consisting in a full body contraction that brings the tip of the tail to the head of the animal. We studied this behavioral response in embryos at 20 hpf. Five embryos at a time were transferred in fish water in a 3.5 mm round petri dish where 5 niches were engraved to host them (Figure 12,A). For each embryo, we evaluated the frequency of spontaneous tail coilings, the percentage of multiple and complex coilings (tail coilings consisting in consecutive repeated bends of the trunk for two or more times, respectively, before returning to the resting condition) and the relative percentage of multiple/complex coilings consisting in alternating left-right bends of the entire body or in tail bends on the same side of the body.

Our analyses revealed that the frequency of spontaneous tail coilings in mSod1 embryos is significantly higher compared to Ctrl ($P = 0.0044$) but not wtSod1 embryos ($P = 0.3404$) (Figure 12,B and Table 19). While the 64.6% of Ctrl and the 66.7% of wtSod1 embryos double the tail bend, the 89.8% of mSod1 embryos perform these multiple tail coilings with a significantly higher percentage, respect to the total amount of tail coilings, compared to both Ctrl ($P = 0.0075$) and wtSod1 ($P = 0.0061$) embryos (Figure 12,C and Table 19). Moreover, while only the 6.25% of Ctrl and the 2.7% of wtSod1 embryos repeat the tail bend more that twice, the 43.5% of mSod1 embryos display complex tail coilings and with a significant higher percentage in comparison with both Ctrl ($P = 0.0003$) and wtSod1 ($P = 0.0002$) embryos (Figure 12,D and Table 19).

Another interesting point observed was that, while Ctrl and mSod1 embryos perform alternating left-right bends of the tail and tail bends on the same side of the body with the same frequency (43.5% of alternate versus 56.5% of same side bends for Ctrl embryos, $P =0.1777$, and 46.2% of alternate versus 53.8% of same side bends for wtSod1 embryos, $P = 0.5423$); mSod1 embryos perform multiple and complex tail bends bringing the tip of the tail on the same side of the body with a significant higher frequency compared to the times they alternate the bends on both sides of the body (36.3% of alternate versus 63.7% of same side bends, $P =0.0005$) (Figure 12,E). No significant differences can be detected in all the parameters took under consideration between Ctrl and wtSod1 embryos.

Table 19

Tail Coilings Analyses	Ctrl	wtSod1	mSod1	P value
Coiling Frequency (Hz)	0.39 ± 0.04	0.50 ± 0.06	0.61 ± 0.05	0.0066
Multiple Coilings (%)	23.24 ± 3.75	21.44 ± 5.20	40.84 ± 4.01	0.0017
Complex Coilings (%)	1.67 ± 1.11	0.80 ± 0.80	11.04 ± 2.84	< 0.0001

Table 19. Spontaneous coilings (Hz), multiple coilings (%) and complex coilings (%) measured in 47 Ctrl, 36 wtSod1 and 46 mSod1 PCR genotyped embryos (see Materials and Methods) embryos. Values are reported as mean ± SEM and were collected in at least 3 independent experiments. We analyzed coiling responses in each embryo for 1 minute and results were statistically analyzed with the software GraphPad Prism® 6.0c version, with One-way Analysis of Variance (ANOVA) or Kruskal-Wallis test and corrected with Tuckey's or Dunn's post-test. The comparison of the relative percentage of alternate versus same side tail bends was performed with Student t test. Means were considered statistically different when P < 0.05. The P values obtained in the statistical analyses are shown.

13. mSod1 EMBRYOS PRESENT ABERRANT TOUCH EVOKED TAIL COILINGS RESPONSES AT 48 hpf

Between 17 and 24 hpf zebrafish embryos do not respond to touch. However, 24 hpf, when the developing sensory system integrates with the motor one, embryos start responding to touch with an over-the-head, fast coiling of the trunk (Brustein et al., 2003). To test touch evoked coiling responses, embryos at 48 hpf, were embedded in a drop of low melting-point-agarose and transferred in a petri dish where they were oriented with the dorsal side up and with the belly facing the bottom of the petri dish. When the agarose solidified, the agarose behind the yolk ball was removed and a drop of fish water was added on the top of the fish. Touch evoked responses were elicited touching the trunk of the embryo, above the yolk ball, with the tip of a microloader (Figure 13,A). For each embryo we measured the duration of the response and the maximum angle of tail flexion (Figure 13,B) in at least 5 responses.

We recorded a significant increase in the duration of the touch evoked responses in mSod1 embryos in comparison to both Ctrl (P = 0.0001) and wtSod1 (P = 0.0053) embryos (Figure 13,B and Table 20) and contemporarily a significant reduction in the maximum angle of tail flexion in mSod1 embryos compared to both Ctrl (P = 0.0004) and wtSod1 (P < 0.0001) embryos (Figure 13,B-C and Table 20). No significant differences can be detected in the two parameters examined between Ctrl and wtSod1 embryos.

Table 20

Touch-evoked Responses Analyses	Ctrl	wtSod1	mSod1	P value
Duration (s)	0.93 ± 0.13	0.88 ± 0.05	3.06 ± 1.03	<0.0001
Maximum Angle of Flexion (°)	86.49 ± 1.67	90.70 ± 2.73	69.47 ± 4.17	<0.0001

Table 20. Duration of the response (s) and maximum angle of flexion (°) measured in 19 Ctrl, 14 wtSod1 and 16 mSod1 embryos screened thanks to DsRed expression after heat shock at 24 hpf (see Materials and Methods). Values are reported as mean ± SEM and were collected in 3 independent experiments. Measures were statistically analyzed with the software GraphPad Prism® 6.0c version, with One-way Analysis of Variance (ANOVA) or Kruskal-Wallis test and corrected with Tuckey's or Dunn's multiple comparison procedure. Means were considered statistically different when P < 0.05.The P values obtained in the statistical analyses are reported.

14. mSod1 LARVAE EXHIBIT ALTERED TOUCH EVOKED SWIMMING ACTIVITY AT 96 hpf

We carried on the study of motor responses in transgenic larvae at 96 hpf, focusing on the analysis of touch evoked swimming responses. To this aim, larvae were individually transferred in a 10 mm petri dish placed on a mesh of 0.5 x 0.5 cm squares (Figure 14,A). Touch evoked swimming responses were elicited touching the trunk of the larvae with the tip of a microloader and were recorded with a digital camera. We measured the duration of the response, the speed and the distance each larva swam in at least 5 responses.

We measured a significant increase in the duration of the swimming response in mSod1 larvae compared to both Ctrl (P = 0.0057) and wtSod1 (P < 0.0001) larvae and in the distance travelled, in each swimming response, by mSod1 larvae compared to Ctrl (P = 0.0204) and wtSod1 (P < 0.0001) fish. We also recorded a significant reduction in the speed of mSod1 larvae compared to both Ctrl (P = 0.0147) and wtSod1 (P < 0.0001) larvae (Figure 14,B and Table 21).

Table 21

Swimming Analyses	Ctrl	wtSod1	mSod1	P value
Response Duration (s)	0.75 ± 0.09	0.77 ± 0.19	3.47 ± 0.94	< 0.0001
Distance Travelled (cm)	1.64 ± 0.22	1.25 ± 0.15	3.47 ± 0.61	0.0001
Speed (cm/s)	2.48 ± 0.11	2.82 ± 0.19	1.88 ± 0.14	0.0001

Table 21. Duration of the response (s), distance travelled (cm) and speed (cm/s) measured in 19 Ctrl, 19 wtSod1 and 19 mSod1 larvae screened thanks to DsRed expression after heat shock at 24 hpf (see Materials and Methods). Values are reported as mean ± SEM and were collected in 3 independent experiments. Results were statistically analyzed with the software GraphPad Prism® 6.0c version, with One-way Analysis of Variance (ANOVA) or Kruskal-Wallis test and corrected with Tuckey's or Dunn's multiple comparison procedure. Means were considered statistically different when P < 0.05.The P values obtained in the statistical analyses are indicated.

15. RILUZOLE TREATMENT REVERTS MOTOR PHENOTYPE AT 20 hpf AND NORMALIZES MOTOR AXONS LENGTH IN mSod1 EMBRYOS AT 24 hpf

Our experiments revealed abnormal motor responses in transgenic embryos and larvae expressing the mutated form of Sod1.

At 20 hpf, mSod1 embryos display an increase in the frequency of spontaneous coiling and show alterations in motor nerves morphology. At this stage of embryonic development, only four types of spinal neurons are active: ipsilateral caudal (IC), ventrolateral descending (VeLD) and commissural primary ascending (CoPA) interneurons and motor neurons (Saint-Amant et al., 2000). They undergo to periodic depolarizations that originate from the activation of pacemaker currents and they are synchronized in a spinal network solely by electrical coupling (Saint-Amant et al., 2001). This represent a unique situation for the study of spinal cord networks development, in fact, this is the only animal model that give us the possibility to study a simple spinal cord functional circuit, capable to give rise to a motor response dependent exclusively on electrical coupling. Moreover, using *in vivo* patch clamp electrophysiology, it has been recently demonstrated that IC interneurons generate inherent bursting activity that depends on a persistent sodium current (I_{NaP}) selectively inhibited by riluzole at low micromolar concentrations (Tong et al., 2012). For all these evidence, we decided to test whether at the basis of this precocious phenotype there was an alteration in the activity of the pacemaker current I_{NaP}. To answer this question, we studied the effect of 5 μM riluzole administration (it has been

demonstrated that at this concentration riluzole selectively inhibits I_{NaP} but no other sodium currents -Tong et al., 2012-) on behavioral responses in embryos at 20 hpf and on motor nerves morphology at 24 hpf.

First of all, we developed a protocol that allowed us to precisely correlate embryos behavioural responses at 20 hpf and spinal nerves morphology at 24 hpf (Figure 15,A). Heterozygous mSod1 zebrafish mating generates a mixed population of transgenic and non-transgenic embryos that cannot be distinguished from each other because they still do not express DsRed (Figure 15,A_A). We performed spontaneous tail coilings analyses placing embryos in the niches engraved in a petri dish paying attention to carefully remove fish water and adding riluzole or vehicle solution (0.2% DMSO) without displacing the embryos from their position (Figure 15,A_B). At the end of the experiment, each fish was individually transferred in a tube, fixed and stained for immunofluorescence and then visualized at the confocal microscope (Figure 15,A_C). When the images acquisition was completed, each fish was singularly collected in a tube, its DNA was extracted and each transgenic fish was identified with PCR thanks to the gene encoding the protein DsRed (Figure 15,A_D).

We observed that riluzole treatment significantly reduced the frequency of spontaneous tail coilings both in Ctrl ($P = 0.0005$) and mSod1 ($P = 0.0471$) embryos compared to the frequency of tail coilings recorded in fish water (Figure 15,B and Table 22). Before riluzole incubation, the 75.0% of Ctrl and the 91.3% of mSod1 embryos performed multiple coilings while, after riluzole administration, only the 17.9% of Ctrl and the 60.9% of mSod1 embryos duplicate tail flexion (Figure 15,B). In addition, riluzole treatment significantly reduced the percentage of multiple tail coilings both in Ctrl ($P < 0.0001$) and in mSod1 ($P = 0.0076$) embryos in comparison to the percentage measured in fish water (Figure 15,B and Table 22).

Riluzole administration produced a terrific effect on complex tail coilings; in fact, while 7.1% of Ctrl and 56.5% of mSod1 embryos did complex tail coilings, after the addition of the drug, only 3.6% of Ctrl and 21.7% of mSod1 embryos still performed complex tail bends (Figure 15,B). Riluzole treatment affected also the relative percentage of alternating left-right bends of the tail versus bends on the same side of the body in mSod1 embryos, in fact, while mSod1 embryos preferentially bent the tail on the same side of the body in fish water (39.5% of alternate bends versus 60.5% of same side bends, $P = 0.0434$), after riluzole treatment, they performed tail bends similarly on both side of the body (46.13% of alternate bends versus 53.87% of same side bends, $P = 0.1862$) (Figure

15,B). Riluzole treatment brought the global spontaneous coiling frequency, the percentage of multiple tail coilings and the type of multiple tail coilings (the relative percentage of alternating and same side tail bends) of mSod1 embryos to levels comparable to those recorded in Ctrl embryos before riluzole administration.

Table 22

	Ctrl		P value	mSod1		P value
	-Riluzole	**+Riluzole**		**-Riluzole**	**+Riluzole**	
Coiling Frequency (Hz)	0.41 ± 0.05	0.22 ± 0.06	0.0005	0.77 ± 0.07	0.51 ± 0.11	0.0471
Multiple Coilings (%)	25.6 ± 4.88	1.30 ± 0.84	<0.0001	49.8 ± 5.56	25.7 ± 6.61	0.0076

Table 22. Spontaneous coiling frequency (Hz) and multiple tail coilings (%) measured in 28 Ctrl, 26 mSod1 embryos in fish water (-Riluzole) and after the administration of fish water containing 5 μM riluzole (+Riluzole). Results were statistically analyzed with unpaired Student t test. Means were considered statistically different when P < 0.05. Values are reported as mean ± SEM and were collected in 4 independent experiments. The P values obtained in the statistical analyses are shown.

To verify the specific effect of riluzole on embryos behavior we performed experiments, with the same experimental procedure described above, incubating embryos with 0.2% DMSO (vehicle) instead of riluzole after spontaneous tail coilings recordings in fish water. Vehicle treatment did not affect spontaneous coiling frequency both in Ctrl and mSod1 embryos (Table 23).

Table 23

	Ctrl		P value	mSod1		P value
	-Vehicle	**+Vehicle**		**- Vehicle**	**+Vehicle**	
Coiling Frequency (Hz)	0.35 ± 0.07	0.38 ± 0.07	0.7429	0.43 ± 0.07	0.44 ± 0.07	0.9497

Table 23. Spontaneous coiling frequency (Hz) measured in 14 Ctrl and 13 mSod1 embryos in fish water (-Vehicle) and after the administration of fish water containing 0.2% DMSO (+Vehicle). Values are reported as mean ± SEM and were collected in 3 independent experiments. Results were statistically analyzed with unpaired Student t test. Means were considered statistically different when P < 0.05. The P values obtained in the statistical analyses are shown.

After recording spontaneous tail coilings in normal fish water or after 10 minutes of riluzole treatment (5 minutes incubation + 5 minutes of movie recording) 24 hpf embryos were fixed and processed for whole-mount fluorescence staining (see Materials and Methods). We acquired z-stacks images of SV2A fluorescence, covering the entire animal trunk in the region comprised by the 12th and the 16th somite. Confocal fluorescence maximum projection images showing SV2A signal were used to measure axonal length, unbranched axonal length and the number of branches with the software ImageJ. Riluzole treatment did not affect either the number of branches or the unbranched axonal length or the number of branches in Ctrl embryos (Figure 15,C and Table 24). However, riluzole administration significantly increased motor axons length in mSod1 embryos without affecting the unbranched axonal length and the number of axonal branches of spinal motor nerves (Figure 15,C and Table 24).

Table 24

	Ctrl		P value	mSod1		P value
	-Riluzole	**+Riluzole**		**-Riluzole**	**+Riluzole**	
Motor Axons Length (µm)	91.5 ± 3.3	88.5 ± 3.6	0.6103	71.44 ± 2.9	82.4 ± 3.8	0.0225
Unbranched Axonal Length (µm)	68.6 ± 3.6	57.9 ± 4.7	0.1139	34.6 ± 2.9	34.04 ± 3.4	0.9030
Number of Branches (n)	2.0 ± 0.2	1.9 ± 0.3	0.8635	4.0 ± 0.2	4.1 ± 0.3	0.8172

Table 24. Motor axons length (µm), unbranched axonal length (µm) and number of branches measured in 28 Ctrl and 33 mSod1 embryos in fish water (-Riluzole) and 10 Ctrl and 22 mSod1 embryos after the administration of fish water containing 5 µM riluzole (+Riluzole). Values are reported as mean ± SEM and were collected in 4 independent experiments. Results were statistically analyzed with unpaired Student t test. The P values obtained in the statistical analyses are shown.

16. mSod1 SPINAL MOTOR NEURONS SHOW MORE FREQUENT SPONTANEOUS DEPOLARIZATIONS

Since I_{NaP} inhibition, through 5 μM riluzole treatment, is able to revert the aberrant motor phenotype and is partially capable to reduce some of the alterations in motor nerves morphology in mSod1 embryos, we decided to assess if at the basis of these precocious alterations there was a change in spinal neurons electrical properties and, in particular, if there were impairments on I_{NaP} mediated spontaneous depolarizations.

Alterations in intrinsic hyperexcitability properties of motor neurons have been observed in neonatal spinal cord organotypic slices (Kuo et al., 2004), neonatal acute brainstem slices (Van Zundert et al., 2008) and dissociated embryonic spinal cord cell cultures (Kuo et al., 2005) from high expressing G93A SOD1 mice and signs of hyperexcitability in motor cortex and surrounding areas have been revealed by electrophysiological studies of ALS patients (Eisen et al., 2002).

We tested whether the aberrant behavioral phenotype observed in mSod1 embryos at 20 hpf, was associated to alterations in the spontaneous depolarizations of spinal neurons, in the intact spinal network of living embryos, using the fluorescence resonance energy transfer (FRET) based voltage biosensor Mermaid (Tsutsui et al., 2008). One-cell stage fertilized eggs, obtained intercrossing AB or mSod1 adult zebrafish, were microinjected with a vector encoding for the biosensor under the control of the pan-neuronal promoter HuC (see Materials and Methods). In this way, we obtained the efficient chimeric expression of the biosensor in a limited population of identifiable neurons in 20 hpf embryos (Figure 16,A) and therefore we managed to study their electrical behavior as FRET Ratio changes (Figure 16,B).

We compared the spontaneous depolarizations detected in Ctrl and mSod1 motor neurons in a minute recording (Figure 16,C) measuring neuronal FRET basal ratio, the frequency of spontaneous depolarizations and the duration and amplitude of each depolarization event.

Our analyses did not reveal any differences in the FRET basal ratio, in the duration and in the amplitude of spontaneous depolarizations between Ctrl and mSod1 embryos, but they highlighted a significant increase in the frequency of spontaneous depolarizations in mSod1 embryos in comparison to Ctrl fish (Figure 16,D and Table 25).

Table 25

	Ctrl	mSod1	P value
Basal Ratio (FRET Ratio)	1.21 ± 0.14	1.54 ± 0.23	0.3258
Frequency (Hz)	0.12 ± 0.02	0.24 ± 0.03	0.0006
Amplitude (FRET Ratio)	0.34 ± 0.05	0.34 ± 0.06	0.9098
Duration (s)	23.7 ± 1.3	25.5 ± 2.6	0.4622

Table 25. Basal ratio (FRET Ratio), frequency (Hz), amplitude (FRET Ratio) and duration (s) of spontaneous depolarizations measured in 12 Ctrl and 12 mSod1 motor neurons. Values are reported as mean ± SEM and were collected in 4 independent experiments. Results were statistically analyzed with unpaired Student t test. Means were considered statistically different when P < 0.05. The P values obtained in the statistical analyses are shown.

17. RILUZOLE ADMINISTRATION DECREASES SPINAL MOTOR NEURONS SPONTANEOUS DEPOLARIZATIONS FREQUENCY

Since Mermaid biosensor proved to be able to detect spontaneous depolarizations in motor neurons, we tested if the treatment with 5 μM riluzole affected this feature in motor neurons. To this aim we recorded the membrane voltage changes of the same motor neuron before and 5 minutes after riluzole solution administration both in Ctrl and mSod1 embryos (Figure 17,A).

We observed that riluzole significantly reduced the frequency of spontaneous depolarizations both in Ctrl and mSod1 embryos without significantly affecting membrane basal FRET ratio and the amplitude and duration of the individual depolarization event (Figure 17,B and Table 26).

Table 26

	Ctrl		P value	mSod1		P value
	-Riluzole	**+Riluzole**		**-Riluzole**	**+Riluzole**	
Basal Ratio (FRET Ratio)	1.21 ± 0.14	1.18 ± 0.26	0.2624	1.54 ± 0.23	1.49 ± 0.31	0.3427
Frequency (Hz)	0.12 ± 0.02	0.04 ± 0.02	0.0031	0.24 ± 0.03	0.12 ± 0.02	0.0126
Amplitude (FRET Ratio)	0.34 ± 0.05	0.22 ± 0.05	0.9098	0.34 ± 0.06	0.27 ± 0.06	0.4288
Duration (ms)	791 ± 44	889± 219	0.5537	863 ± 86	1094 ± 215	0.2842

Table 26. Basal ratio (FRET Ratio), frequency (Hz), amplitude (FRET Ratio) and duration (ms) of spontaneous depolarizations *measured in 12 Ctrl and 12 mSod1 motor neurons before and after riluzole administration. Values are reported as mean ± SEM and were collected in 4 independent experiments. Results were statistically analyzed with unpaired Student t test. The P values obtained in the statistical analyses are shown.*

18. SPINAL INTERNEURONS PRESENT DIFFERENT PATTERNS OF MEMBRANE VOLTAGE CHANGES AND DIFFERENTLY RESPOND TO RILUZOLE TREATMENT

One of the advantages of our experimental approach is the possibility to characterize the membrane voltage properties of any kind of neuron, recognized thanks to its peculiar morphology. We therefore investigated not only motor neurons electrical properties but also those of spinal interneurons before and after riluzole administration, in the same developmental window, when neuronal networks exist only through electrical coupling.

In Ctrl and mSod1 embryos we classified spinal interneurons in three different classes according to their patterns of depolarization (Figure 18,A-B): a first group of interneurons does not present spontaneous depolarizations either before or after riluzole treatment (hereafter referred as Type 0 interneurons), a second class displays spontaneous depolarizations in basal conditions and its voltage membrane activity is affected by riluzole treatment (hereafter referred as Type 1 interneurons), and a third group does not show spontaneous depolarizations before riluzole administration but develops a spontaneous depolarization activity after the incubation with riluzole (hereafter referred as Type 2 interneurons). In Ctrl embryos the majority of interneurons (66%) did

not show periodic depolarization and their electrical properties did not change after riluzole treatment (Type 0). The remaining interneurons (34%) displayed periodic depolarizations before riluzole treatment in the 75% of cases (Type 1) and only after riluzole treatment in the 25% of cases (Type 2) (Figure 18,A). Also in mSod1 embryos most interneurons (67%) did not show periodic depolarizations either before of after riluzole treatment (Type 0). Other interneurons (33%) underwent to periodic depolarization before riluzole treatment in the 73% (Type 1) of cases and only after riluzole treatment in the 27% of cases (Type 2).

19. mSod1 EMBRYOS SPINAL INTERNEURONS SHOW MORE FREQUENT SPONTANEOUS DEPOLARIZATIONS THAT DECREASE AFTER RILUZOLE TREATMENT

Since we wanted to understand if the alteration in the spontaneous depolarizations frequency was a peculiar motor neurons phenotype or if a change in the depolarization pattern affected the entire spinal network, we compared the basal ratio and the spontaneous depolarization frequency measured in motor neurons with those recorded in Type 1 interneurons. We subsequently compared the effects of riluzole administration in Ctrl and mSod1 Type 1 interneurons with those observed in motor neurons with the aim of understanding if riluzole reduced motor neurons depolarizations frequency acting on the entire network or exerting its effect on a specific neuronal subtype.

We did not detect any differences in the basal ratio calculated in motor neurons and in Type 1 interneurons before riluzole treatment both in Ctrl ($P = 0.5356$) and mSod1 ($P= 0.9736$) embryos. The mean basal FRET ratio after riluzole administration did not differ between motor neurons and interneurons in Ctrl ($P = 0.6445$) and mSod1 ($P = 0.5290$) embryos. Also the frequency of spontaneous depolarizations is comparable in motor neurons and interneurons in Ctrl and mSod1 embryos before ($P = 0.6996$ and $P = 0.5223$ for Ctrl and mSod1, respectively) and after ($P = 0.6897$ and $P = 0.7421$ for Ctrl and mSod1 respectively) riluzole administration (Figure 19,A).

We further studied the basal FRET ratio and the frequency of spontaneous depolarizations in Type 1 and Type2 interneurons before and after the substitution of fish water with water containing riluzole in Ctrl and mSod1 embryos (Figure 19,B and Tables 27 and 28).

Ctrl and mSod1 Type 1 interneurons did not show significant differences in the basal FRET ratio before riluzole treatment ($P = 0.0536$) and did not change their basal

ratio after the drug administration (Table 27). Type 1 interneurons of mSod1 embryos, however, present a significant higher frequency of spontaneous depolarizations compared to that of Ctrl embryos (P = 0.0210). In both cases riluzole significantly reduced the frequency of spontaneous depolarizations (Table 27).

Type 2 interneurons of mSod1 embryos did not display significant differences in the basal FRET ratio in comparison to Ctrl embryos (P = 0.0714) in basal conditions. However, riluzole treatment tends to slightly modify basal FRET ratio (Table 28) both in Ctrl and mSod1 embryos, probably favoring the comparison of spontaneous depolarizations in Type 2 Ctrl and mSod1 interneurons at comparable frequency (P = 0.5714) (Table 28).

Table 27

	Ctrl		P value	mSod1		P value
	-Riluzole	+Riluzole		-Riluzole	+Riluzole	
Basal Ratio (FRET Ratio)	1.01 ± 0.05	1.22 ± 0.28	0.6667	1.83 ± 0.39	1.83 ± 0.52	0.5573
Frequency (Hz)	0.11 ± 0.03	0.01 ± 0.01	0.0086	0.22 ± 0.03	0.12 ± 0.03	0.0150

Table 27. Basal ratio (FRET Ratio) and frequency (Hz) of spontaneous depolarizations measured in 5 Ctrl and 16 mSod1 Type 1 interneurons before and after riluzole administration. Values are reported as mean ± SEM and were collected in 4 independent experiments. Results were statistically analyzed with unpaired Student t test and means were considered statistically different when P < 0.05. The P values obtained in the statistical analyses are shown.

Table 28

	Ctrl		P value	mSod1		P value
	-Riluzole	+Riluzole		-Riluzole	+Riluzole	
Basal Ratio (FRET Ratio)	0.45 ± 0.22	1.06 ± 0.83	0.6667	1.62 ± 0.37	1.24 ± 0.28	0.1667
Frequency (Hz)	0.00 ± 0.00	0.18 ± 0.04	0.3333	0.00 ± 0.00	0.20 ± 0.02	0.0022

Table 28. Basal ratio (FRET Ratio) and frequency (Hz) of spontaneous depolarizations measured in 2 Ctrl and 6 mSod1 Type 2 interneurons before and after riluzole administration. Values are reported as mean ± SEM and were collected in 4 independent experiments. Results were statistically analyzed with unpaired Student t test and means were considered statistically different when P < 0.05. The P values obtained in the statistical analyses are shown.

Finally, we checked for alterations in amplitude and duration of spontaneous depolarizations in Type 1 interneurons before and after riluzole treatment in Ctrl and mSod1 embryos. As in motor neurons, we did not observe any differences both in amplitude (P = 0.6820) and duration (P = 0.6570) of depolarizations between Ctrl and mSod1 embryos in basal conditions and also after riluzole administration (Figure 19,C and Table 29).

Table 29

	Ctrl		P value	mSod1		P value
	-Riluzole	**+Riluzole**		**-Riluzole**	**+Riluzole**	
Amplitude (FRET Ratio)	0.37 ± 0.07	0.22 ± 0.01	0.0961	0.33 ± 0.08	0.23 ± 0.07	0.4396
Duration (ms)	692.4 ± 56.8	557.7 ± 47.02	0.1427	759.8 ± 131.9	821.4 ± 114.2	0.7335

Table 29. Amplitude (FRET Ratio) and duration (ms) of spontaneous depolarizations measured in 5 Ctrl and 5 mSod1 Type 1 interneurons before and after riluzole administration. Values are reported as mean ± SEM and were collected in 4 independent experiments. The number of analyzed neurons is reported in brackets. The P values obtained in the statistical analyses are shown.

DISCUSSION

In this present study, in which we propose zebrafish as an animal model for the study of ALS, we have performed the detailed characterization of ALS features occurring in transgenic zebrafish models overexpressing mutant Sod1 G93R (mSod1) and wild-type Sod1 (wtSod1).

In the adult zebrafish models, we have studied most of the main pathological events occurring in ALS, that have already been described in humans and other animal models of the disease: locomotor impairments, motor neurons degeneration, spinal cord and muscular atrophy, neuromuscular junctions loss and ultrastructural alterations in the nerves terminals and muscles. Furthermore, in these zebrafish models, we have assessed the involvement of astrocytes, microglia and peripheral inflammatory cells in the disease pathogenesis. In order to identify the defects associated with the disease and how these defects affect the entire trunk of the animal, we have mapped these events along the entire body of the animal.

Following the characterization of the disease profile in adult zebrafish, we have searched for precocious ALS-related hallmarks in zebrafish embryos and larvae studying how the overexpression of the wild-type or mutant Sod1 affects spinal motor neurons development and neuromuscular junctions maturation. We have performed behavioral tests in order to examine changes in motor activity on zebrafish embryos and larvae and we have investigated spinal motor neurons and interneurons electrical properties of mSod1-expressing zebrafish embryos. Finally, we have examined the possibility of pharmacological modulation of precocious alterations associated to the mutant Sod1 expression by administering riluzole directly into the embryo water.

1. ADULT Sod1 G93R ZEBRAFISH DISPLAY TYPICAL NEUROMUSCULAR FEATURES OF ALS

Zebrafish generally have a life expectancy of 2-3 years in zebrafish facilities and at 12 months they are adults far from the pathological end-stage of ALS that has been reported to occur after 18 months (Ramesh et al., 2010). We started the characterization of Sod1 overexpressing zebrafish studying the effects of wild-type Sod1 or mutant Sod1 expression on zebrafish macroscopic anatomy at 12 months of age. The expression of either the wild-type or mutant Sod1 does not affect the standard length, the height at anterior of anal fin, the length from the operculum to the caudal peduncle and the body weight of adult zebrafish. These observations are in agreement with those obtained from

studies of mice expressing mutant SOD1. In fact, although a slowing of growth roughly two weeks preceding the onset of motor symptoms has been reported, SOD1 mice maintain a normal weight range in comparison with non-transgenic littermates and it is only within the last 2 weeks of their illness that they loose up to 10% of their body weight, mostly due to paralysis which prevents them from feeding (Chiu et al., 1995; Fischer et al., 2004). Twelve months old mutant zebrafish however, do not have such severe swimming impairments as to compromise their capability to feed and do not exhibit a weight loss.

As in patients (Vucic et al., 2014 and references therein) and rodent models of ALS (Turner & Talbot 2008 and reference therein; Vinsant et al., 2014a-b) Sod1 G93R expressing zebrafish present motor abnormalities. Beside the endurance impairment previously observed in swimming against increasing water current flow rate (Ramesh et al., 2010); 12 months old mSod1 zebrafish show a significant reduction in the distance travelled and an increase in the time spent at resting in the spontaneous locomotor activity in comparison to control fish. The increase in the time spent in the "resting" phase during the spontaneous swimming was also observed in the SOD1 G93A zebrafish model (Sakowski et al., 2012) and in the Sod1 T70I zebrafish model (Da Costa et al., 2014). Interestingly, the SOD1 G93A zebrafish model exhibits a consistently lower swimming velocity relative to age-matched AB control along the entire disease course; however, this reduction is never significant (Sakowski et al., 2012) and this is similar to what we detected in our model that does not show a significant reduction in the swimming speed.

Motor neurons loss is one of the hallmark features of ALS; however, it is a late stage event occurring in ALS pathogenesis. Several studies, performed on mice models, reported a significant loss of somatic motor neurons of the spinal cord by 90 days of age, at the onset of clinical symptoms (Chiu et al., 1995; Fischer et al., 2004). However, it has been recently reported that SOD1 G93A expressing mice, start loosing motor neurons between P60 and P75, motor neurons death seems to be heralded by cytoplasmic vacuolization beginning between P44 and P60 and the total motor neurons loss observed by the pathology end stage is approximately 50% (Vinsant et al., 2014b). Histological analyses showed that, at 12 months of age, when Sod1 G93R zebrafish display the motor impairment, they present a significant reduction in spinal cord area and in the number of spinal motor neurons compared to both control and wtSod1 zebrafish. Interestingly, in this model, motor neurons loss and spinal cord atrophy uniformly affect the entire trunk while, in the mouse model, the reduction of cholinergic neurons was restricted to the ventral horns of cervical and lumbar spinal cord while no significant reduction in somatic motor

neurons innervating axial muscle located at the thoracic level was recorded (Chiu et al., 1995). It is worth noting that, also this model shares peculiar ultrastructural alterations in spinal cord motor neurons. At pathology end stage, the ultrastructural analyses revealed shrunken spinal motor neurons containing vacuolated mitochondria with disorganized cristae (Ramesh et al., 2010).

A more precocious event in ALS pathogenesis is the loss of the synaptic contacts between motor neurons and muscle fibers. In mice expressing high levels of human SOD1 G93A, many neuromuscular junctions are lost in tibialis anterior and gastrocnemius muscles from 47 postnatal days on; before any detectable losses of motor neurons in the spinal cord and long before any clinical sign of the disease (Frey et al., 2000; Fischer et al., 2004; Gould et al., 2006; Hegedus et al., 2008).

The Sod1 G93R zebrafish model, at 12 moths of age, together with motor neurons loss, displays the reduction of the 50% of neuromuscular connections in the white lateral muscles of the trunk. Such a reduction in the percentage of innervation of postsynaptic specializations seems to be the effect of presynaptic terminals degeneration because we observed a significant reduction only in the density of presynaptic clusters but not of postsynaptic clusters in mSod1 musculature. Interestingly, surviving pre and postsynaptic clusters of mSod1 zebrafish are not different in their size or in the fluorescence intensity signal associated. The preservation of residuals presynaptic boutons is further demonstrated by the ultrastructural analysis of adult zebrafish neuromuscular junctions in the white lateral muscles of mSod1 zebrafish, in fact, they do not present any peculiar morphological alterations (data not shown). This is in agreement with the same investigations performed in SOD1 G93A mice models were only a few subset of neuromuscular boutons present ultrastructural alterations at disease onset (Cappello et al., 2012; Vinsant et al., 2014b).

The reason why such a pronounced denervation is associated to a mild locomotor impairment could be explained by the fact that zebrafish white lateral muscle fibers are polyinnervated; in fact, each fast fiber is innervated by a single primary motor neuron and up to 4 secondary motor neurons (Babin et al., 2014). This means that the white muscle fibers completely lacking a neuromuscular contact are probably fewer than the 50%. Moreover, the slow sustained swimming that mainly contributes to the spontaneous swimming activity is largely mediated by slow fibers contraction. Slow fibers form a thin superficial layer on the surface of the myotome, are well-equipped for oxidative phosphorylation and are therefore resistant to fatigue, fast fibers, on the contrary, only

become active during rapid swimming or escape movements (Drapeau et al., 2002; Brustein et al., 2003). Since electrophysiological evidence indicate that slow fibers are tonic fibers, homologous to the tonic fibers described in the mammalian extra-ocular muscle and these fibers are generally spared by the disease in human patients (Kiernan et al., 2011) we could also hypothesize that red fibers are significantly spared by denervation thus contributing to the maintenance of the zebrafish spontaneous swimming activity.

Skeletal muscle is one of the tissues affected both in sporadic and familial human ALS beside the central nervous system. Both, patients and mouse models expressing mutant SOD1, present functional aberrations and skeletal muscle symptoms (Boyer at al., 2013 and references therein). Mutant Sod1 zebrafish display a significant reduction in the mean white fibers caliber compared to control zebrafish, along the entire trunk, particularly severe in the most caudal portion of the body wall. We examined the ultrastructure of adult white muscle fibers of zebrafish trunk with the electron microscope. Particularly, we focused our attention to the ultrastructural organization of sarcomeres and performed the morphometric analyses of muscular mitochondria measuring their area, perimeter and circularity in control fish and mSod1 zebrafish. Although we did not observe any alteration in the organization of the contractile apparatus as it was reported previously at the pathology end stage (Ramesh et al., 2010); preliminary results obtained analyzing more than 100 mitochondria in one animal per genotype evidenced a significant reduction in the area, perimeter and circularity of muscular mitochondria in mSod1 zebrafish compared to control zebrafish without other defects in mitochondria ultrastructure (cristae disorganization or swelling). Also in this case, this model recapitulates one of the disease features already identified in other models, in fact, the ubiquitous expression of zinc-deficient SOD1 in *Drosophila* deteriorates mitochondrial structure causing cristae rearrangement (Bahadorani et al., 2013). Mitochondrial morphological alterations and dysfunction have been observed also when mutant SOD1 in mouse is expressed only in muscle fibers (Dobrowolny et al., 2008).

2. ADULT Sod1 G93R ZEBRAFISH PRESENT ASTROGLIOSIS AND ACTIVATED INFLAMMATORY CELLS INFILTRATION IN LATERAL MUSCLE

Several studies, performed in both humans and mice, have shown that glial cells, which surround motor neurons and provide them with nutritional and trophic support, could

play a crucial role in disease pathogenesis. Since the contribution of glial cells in the zebrafish pathology has never been addressed, we investigated the involvement of astrocytes and microglia to ALS pathogenesis in the spinal cord of our G93R zebrafish model.

Astrocytes respond to all forms of injury in a typical manner known as reactive astrogliosis mediated by the activation of resident astrocytes and by a change in their proteins expression, for instance increasing the expression of the protein GFAP and altering the morphology of their cellular processes. We performed immunofluorescence experiments with antibodies against the zebrafish protein Gfap to evaluate if along zebrafish spinal cord we could identify reactive astrogliosis as it has been observed in ALS patients and other ALS-animal models (Philips & Rothstein, 2014 and references therein).

We measured a significant increase in Gfap fluorescence signal in the spinal cord of both mSod1 and wtSod1 adult zebrafish, particularly pronounced in the last segments (S4-S5) of the spinal cord. This result is extremely interesting because it has been shown that astrogliosis gradually increases with disease progression not only in mutant SOD1 expressing mice but also in those expressing wild-type SOD1 at comparable levels at 40, 80 and 120 postnatal days (Alexianu et al., 2001).

In ALS patients, as well as in ALS rodent models, there is also a clear microglial reaction characterized by the up regulation of a whole range of microglial markers (CD11b, IBA1) and by the release of pro-inflammatory cytokines and chemokines (Philips & Rothstein, 2014 and references therein).

In our transgenic animals, however, the measurement of the mean fluorescence signal per spinal cord μm^2, after the immunofluorescence staining against the microglial marker Aif1 (the zebrafish homolog of IBA1), did not show any significant differences among zebrafish of the three genotypes despite a remarkable increase of the signal toward the most caudal segments of the spinal cord in mSod1 and wtSod1 zebrafish. We can hypothesize that a higher increase in microglial activation could appear at later stages during disease pathogenesis; in fact, either mutant SOD1 G93A or wild-type SOD1 transgenic mice do not show increase in activated microglia in the spinal cord at 40 days of age (stage at which astrocytosis is already present); however, at 80 days, extensive staining for microglia was observed in the ventral horn and proximal part of the anterior roots (Alexianu et al., 2001). Moreover, the analysis of microgliosis in the central nervous system of ALS patients, which demonstrated increased microgliosis in the motor cortex, in the motor nuclei of the brain stem, in the corticospinal tract and in the ventral horn of the spinal cord largely depends on

studies of postmortem tissues (Kawamata et al., 1992). It is also important to stress that microgliosis in ALS patients is more prominent in motor cortex than in the spinal cord and it has been detected a high correlation between the extent of microgliosis and the damage to upper motor neurons but not to the damage of lower motor neurons (Turner et al., 2004) supporting a less prominent microglial activation in the spinal cord.

The immunofluorescence staining against Aif1 revealed a significant enrichment of activated macrophages and neutrophils around atrophic muscular fibers in mSod1 zebrafish white lateral muscle, compared to both wtSod1 and Ctrl zebrafish.

This observation is very interesting because also mice expressing either mutant SOD1 G93A or SOD1 G37R present a wide infiltration of macrophages in the peripheral nervous system accompanying axons degeneration in ventral roots, sciatic nerves, and muscle tissues (Chiu et al., 2009; our unpublished results). Therefore, we could hypothesize that, also in this model, the denervation of the peripheral nervous system and the degeneration of motor axons lead to significant peripheral macrophage activation; in fact, macrophages in ALS transgenic mice are mainly derived from the circulation and their primary role in peripheral nerves is the phagocytic removal of debris following axonal degeneration (Chiu et al., 2009). As it has been observed in mice, where a huge macrophage activation occurs only in mutant SOD1 expressing mice, but not in non transgenic and wild-type SOD1 expressing mice (Chiu et al., 2009), the significant increase in activated inflammatory cells was detected only in mutant Sod1 expressing zebrafish.

3. ADULT Sod1 TRANSGENIC ZEBRAFISH RECAPITULATE THE MAIN PATHOGENETIC EVENTS ASSOCIATED TO SOD1 OVEREXPRESSION

The characterization of the adult zebrafish overexpressing the mutant *sod1* G93R gene reveals that this model recapitulate most of the main pathogenetic hallmarks studied in other animal models of ALS expressing SOD1 mutations (Turner & Talbot, 2008).

When motor impairments in spontaneous swimming activity become detectable, we observed a significant loss of motor neurons and spinal cord atrophy along the entire trunk of the animals. This spinal motor neurons loss surely occurs during ALS progression and is not due to a defect in spinal cord neurogenesis because we did not detected any

reduction in the number of spinal motor neurons in mutant embryos, stained with antibodies against acetylated tubulin, at 24 hpf (data not shown).

This phenotype is comparable to that observed in mice expressing SOD1 mutations at 80-90 postnatal days when they show the first consistent clinical sign of disease: a fine shaking or tremor occurring in one or more limbs. The onset of clinical symptoms in mutant mice represents also the disease stage at which a significant loss of somatic motor neurons from the cervical (C7) and lumbar (L7) segments of the spinal cord is observed (Chiu et al., 1995).

In mutant SOD1 mice models motor neurons loss follows neuromuscular junctions degeneration, which can be detected from 47 postnatal days on (Frey et al., 2000; Fischer et al., 2004; Gould et al., 2006; Hegedus et al., 2008), and skeletal muscle atrophy (Fischer et al., 2004). In the G93R zebrafish model we detected a severe denervation and atrophy of white muscle fibers that possibly started much earlier than at 12 months of age. To support this hypothesis, we performed histological analyses in 3 zebrafish for each genotype at 7 months of age. The preliminary data collected to date show already a significant severe reduction of white muscle fibers caliber, spinal cord atrophy and motor neurons loss in mSod1 zebrafish compared to control zebrafish, although not as prominent as at 12 months of age. However, 7 months old mSod1 zebrafish do not show signs of reactive astrogliosis or microgliosis in the spinal cord or the presence of activated inflammatory cells in the white lateral musculature. Therefore, one of our future aims will be to further confirm these data, particularly focusing on the study of the degree of innervation at this age in order to evaluate if also this model could support a “dying back” process at the basis of ALS pathogenesis.

It is also important to point out that also in this animal model the overexpression of the wild-type form of Sod1 is associated to the development of mild alterations. Although wild-type Sod1 overexpression does not affect adult zebrafish macroscopic anatomy and motor neurons survival, it is associated to a slight reduction in locomotor performance and white muscle fibers caliber, although they are never significantly different from those of control fish. Even in this case, these observations, are similar to those obtained studying transgenic mice overexpressing wild-type SOD1 were these mice present hypotonia, hindlimb neuromuscular pathology and even muscular dystrophy (Turner & Talbot, 2008 and references therein). Moreover, wild-type SOD1 overexpression in G93A mice causes a significant increase in spinal cord astrogliosis at comparable levels to that observed in

mutant SOD1 expressing mice (Alexianu et al., 2001) as we observed in the spinal cord of wild-type Sod1 expressing zebrafish.

4. MUTANT Sod1 EXPRESSION PRECOCIOUSLY AFFECTS MOTOR SYSTEM MORPHOLOGY

The most common alteration observed in zebrafish expressing mutant genes associated to ALS is a motor axonopathy at early developmental stages. Abnormal branching and reduced length of spinal motor neurons axons was reported in embryos microinjected with RNA encoding for different human mutant SOD1: SOD1 G93A, SOD1 G37R and SOD1 A4V at 30 hpf (Lemmens et al., 2007; Sakowski et al., 2012). These defects have been also observed after the down regulation or the transient expression of other genes involved in ALS, in fact, both the knockdown of C9orf72 and the transient overexpression of mutant TARDBP and FUS cause aberrant branching and a significant reduction in the axonal length and in the unbranched axonal length of motor nerves in zebrafish embryos at 24, 48 or 72 hpf (Ciura et al., 2013; Kabashi et al., 2010b; Kabashi et al., 2011).

Sod1 G93R expressing embryos display a significant reduction both in the motor axons length and in their unbranched axonal length and they shows a significant increase in the number of motor nerves axonal branches compared to Ctrl embryos, along the entire trunk already at 24 hpf. While the reduction in motor axons length is comparable to that observed previously (Lemmens et al., 2007), the increase in the mean number of branches per motor nerve counted in our model is consistently less important. This may be due to both the precocious developmental stage studied (24 hpf Vs 30 hpf) and the higher transgene expression level obtained by RNA microinjection. Interestingly this phenotype was no longer present at later stages of embryos development.

At this developmental stage, also zebrafish embryos overexpressing the wild-type form of Sod1 show a significant reduction in both the motor axons length and in their unbranched axonal length in comparison to control embryos, similarly to what observed in mSod1 embryos; however they do not show aberrant branching. We could hypothesize that these effects may be associated to the toxicity associated to the overexpression of the wild-type form of Sod1 already reported in mice (Dal Canto & Gurney 1995; Jaarsma, 2006; Turner & Talbot, 2008) and other animal models (Watson et al., 2008) on motor axons outgrowth; a process that has been demonstrated to be particularly sensitive to the

down or up-regulation of a number of proteins (Kabashi et al., 2010a; Kabashi et al., 2011; Kabashi et al., 2013; Ciura et al., 2013). The potential toxicity of wild-type Sod1 overexpression at precocious developmental stages was already suggested by previous experiments showing that the 30% of SOD1 WT microinjected embryos presented axonal outgrowth abnormalities and also that the co-microinjection of SOD1 WT with SOD1 A4V exacerbates the toxic effect on motor axons length mediated by the overexpression of SOD1 A4V alone (Lemmens et al., 2007).

At 48 hpf, we analyzed another crucial target of the pathology, the neuromuscular junction. Particularly, we investigated the presence of precocious impairments in the development of synaptic contacts between motor axons and muscle fibers caused by mSod1 expression. We did not observe differences in the density of developing presynaptic vesicle clusters, distributed along spinal motor axons, in the density of AChRs postsynaptic clusters forming on muscle precursors plasmamembrane and in the density of pre and postsynaptic superimposing (colocalizing) clusters among zebrafish of the three genotypes. Although the dimension of AChRs clusters, whose formation is independent from any neuronal stimulus in this developmental phase, is comparable among embryos (Panzer et al., 2005 and reference therein), we measured a significant increase in the dimension of synaptic vesicle clusters in mSod1 embryos compared to Ctrl and wtSod1. Since this phenotype seems associated to an increased persistency of vesicles along the main neuronal axon and newly formed branches, instead of being delivered and efficiently clustered at the tips of axonal branches, we could speculate that this increase in cluster dimension may be due to a delay in synaptic vesicles delivery to axonal tips because of defects in anterograde axonal transport (De Vos et al., 2007).

This precocious impairment in neuromuscular contacts maturation gets worse as development proceeds. At 96 hpf, while the dimension of synaptic vesicles and AChRs clusters result similar among transgenic and non-transgenic larvae, observations confirmed by the ultrastructural analyses; we measured a significant reduction in the density of presynaptic clusters in mSod1 larvae musculature compared to both Ctrl and wtSod1 larvae without alterations in the density of AChRs postsynaptic clusters. Moreover, we detected a significant reduction in the association of presynaptic and postsynaptic clusters in mSod1 embryos compared to both wtSod1 and Ctrl fish highlighting a severe impairment in neuromuscular junctions formation at this precocious developmental stage. Similar observations were detected in zebrafish larvae, at 50-54 hpf, transiently expressing a mutant form of FUS protein or in zebrafish with knockdown of FUS, which displayed a

higher number of both presynaptic orphan puncta and postsynaptic orphan clusters when compared with wild-type larvae and larvae expressing wtFUS. With electrophysiological recordings, it was also demonstrated that significant presynaptic defects occurred at these neuromuscular junctions in fact, they showed a significant reduced frequency of miniature endplate currents (Armstrong & Drapeau, 2013).

Although precocious defects in neuromuscular junctions have already been reported in Sod1 G93R (Ramesh et al., 2010) and Sod1 T70I (Da Costa et al., 2013) zebrafish larvae at 11 dpf and in adult zebrafish expressing Sod1 G93R (Ramesh et al., 2010) and SOD1 G93A (Sakowski et al., 2013), this issue has never been address systematically, so precociously during development. These data, in fact, suggest specific toxic effects of mutant Sod1 expression already during the establishment of neuromuscular contacts and not only a detrimental effect of the mutant protein on neuromuscular junction maintenance in the adulthood.

Given the precocious defects observed in motor axons outgrowth and neuromuscular junctions maturation, we also investigated if muscle fibers were damaged by mSod1 expression in larvae at 96 hpf. We exploited the advantages of zebrafish optical transparency and the capability to detect myosin SHG signal, generated by larvae intact muscles, to measure fibers caliber and study myofilaments organization. We measured a significant reduction in muscle fibers caliber in mSod1 larvae compared to control larvae but the preservation of the organization and of the fine structure of the contractile apparatus. Ultrastructural analyses also revealed that sections of mitochondria of mutant larvae muscle fibers were altered with a significant reduced area, as already seen in adult muscles, confirming that also in this model mitochondria represent precocious targets of the disease (Dupuis et al., 2003).

5. Sod1 G93R EXPRESSION LEADS TO PRECOCIOUS MOTOR ABNORMALITIES

Recent studies have shown that the knockdown or the transient expression of ALS related genes are associated to the appearance of motor impairments early during development. Forty-eight hpf zebrafish embryos injected with mutant TARDBP RNAs or with *tardbp* antisense morpholino oligonucleotides (AMO) showed deficit in the swimming response evoked by touch, in particular, they were unable to swim away following a touch, even though they were sensitive to touch (Kabashi et al., 2010b). The knockdown of the *zc9orf72* orthologue in 96 hpf zebrafish larvae caused a deficient touch evoked escape

response with a reduction in the total distance travelled and in the average and maximum velocity of the locomotor behavior and a reduced motility in the spontaneous swimming assay (Ciura et al., 2013). Forty-eight hpf zebrafish embryos knocked down for the expression of the zebrafish homologue of VAPB displayed a defective escape response at 48 hpf when lightly touched on the tail while, wild-type larvae, following touch, exhibited robust escape responses, characterized by swimming away from the tactile stimuli for a few seconds (Kabashi et al., 2013). Larvae expressing the human FUS R521H missense mutation and larvae injected with the AMO against zebrafish *fus* respond to touch, eliciting a bout of swimming but fatigued quickly, displaying shorter swim duration when compared with wild-type larvae (Armstrong & Drapeau, 2013).

Given all these data, we decided to analyze motor behavior in embryos and larvae expressing mutant and wild-type Sod1. We studied spontaneous coiling in 20 hpf embryos and we detected a significant increase in the frequency of spontaneous tail coilings in mSod1 embryos. They displayed an overall increased motility characterized by a significantly higher percentage of multiple and complex tail coilings compared to both Ctrl and wtSod1 embryos. Moreover, while Ctrl and wtSod1 embryos perform alternated left-right tail bends of the tail and tail bends on the same-side of the body with the same frequency, mSod1 embryos performed multiple and complex same-side tail bends with a significant higher frequency compared to those alternate. We kept on studying embryos motility at 48 hpf, when we observed that mSod1 embryos exhibited a significant increase in the duration of the touch evoked tail coilings responses and a significant decrease in the maximum angle of tail flexion compared to Ctrl and wtSod1 embryos and even at 96 hpf mSod1 larvae preformed significantly prolonged evoked swimming responses travelling a higher distance in comparison to Ctrl and wtSod1 fish. Since these responses, in mSod1 larvae, consist in repeated consecutive burst swimming events, the overall speed of mSod1 responses results significantly lower compared to Ctrl and wtSod1 fish. In every circumstance, wtSod1 embryos and larvae do not show different motor behaviors in comparison with control fish.

Our observations significantly contrast with the effects of the overexpression or down-regulation of ALS associated genes that appear to reduce the motility of zebrafish embryos and larvae. In fact, we actually observed an increase in motility during all the developmental stages studied. Given this inconsistency, we next sought to determine whether the basis of this overall increase in motility could be related to altered spinal neurons electrical properties.

6. EMBRYOS EXPRESSING mSod1 DISPLAY INCREASED SPINAL NEURONS EXCITABILITY

Thanks to the FRET-based voltage biosensor Mermaid, we investigated spontaneous depolarizations in spinal interneurons and motor neurons in the zebrafish intact locomotor network.

At 20 hpf, only four types of spinal neurons are active: ipsilateral caudal (IC), ventrolateral descending (VeLD) and commissural primary ascending (CoPA) interneurons and motor neurons (Saint-Amant et al., 2000). They undergo periodic depolarizations that originate from the activation of pacemaker currents and they are synchronized in a spinal network solely by electrical coupling (Saint-Amant et al., 2001). In agreement with that, we recorded spontaneous depolarizations in embryonic spinal motor neurons and in a small portion (33-34%) of the interneurons analyzed in both Ctrl and mSod1 embryos.

In mutant embryos both motor neurons and interneurons showed a significant increase in the frequency of spontaneous depolarizations but no changes in the FRET basal ratio or in the amplitude and duration of each individual depolarization event compared to Ctrl embryos. The fact that not only motor neurons but also interneurons displayed a comparable increase in the frequency of spontaneous depolarizations, suggest that in mutant embryos the entire locomotor network displays an elevated intrinsic electrical excitability.

These results are extremely relevant since several studies demonstrated that ALS patients exhibit cortical hyperexcitability before any clinical sign of ALS (Vucic et al., 2008; Vucic et al., 2013b; Menon et al., 2014). Moreover, these data are in agreement with studies performed in cultured mice embryonic and neonatal dissociated spinal motor neurons expressing mutant SOD1 G93A. SOD1 G93A expressing neurons did not show any differences in the resting potential, in the input conductance, in the action potential shape and in the after hyperpolarization amplitude in comparison to control motor neurons; however, their maximal firing rate was much greater than in the control ones also in the presence of ionotropic receptors blockers in order to assure that these differences were not due to alterations in spontaneous synaptic inputs (Kuo et al., 2004; Pieri et al., 2009; Schuster et al., 2012; Martin et al., 2013). Similar results were obtained comparing hypoglossal motor neurons and spinal cord interneurons electrical properties of mutant human SOD1 G93A expressing mice with those recorded in wild-type human SOD1 expressing mice and non-transgenic mice in acutely prepared slice at P4-P10 or P10-P12.

In this way, it was demonstrated that neuronal hyperexcitability was specifically due to the expression of the mutated SOD1 G93A protein but not of wild-type SOD1 and that even interneurons present hyperexcitability, which may contribute to neuronal loss at later stages in the pathology (Van Zundert et al., 2008).

Since, using *in vivo* patch clamp electrophysiology, it has been recently demonstrated that IC interneurons generate intrinsic spontaneous depolarizations that depends on a persistent sodium current (I_{NaP}) selectively inhibited by riluzole at low micromolar concentrations in embryos between 17 and 24 hpf (Tong et al., 2012), we decided to test whether at the basis of this increased neuronal excitability there was an alteration in the activity of the pacemaker current I_{NaP}. To answer this question, we studied the effect of 5 μM riluzole administration, a concentration that selectively inhibits I_{NaP} but no other sodium currents (Tong et al., 2012) on neuronal spontaneous depolarizations and ultimately on behavioral responses in embryos at 20 hpf and on motor nerves morphology at 24 hpf.

7. RILUZOLE REDUCES SPINAL NEURONS HYPEREXCITABILITY, REVERTS ABERRANT COILING BEHAVIOR AND NORMALIZES MOTOR AXONS LENGTH IN mSod1 ZEBRAFISH EMBRYOS

The incubation of 20 hpf mSod1 embryos with riluzole did not affect motor neurons and interneurons basal FRET ratio or amplitude and duration of periodic depolarizations but, significantly reduced the frequency of depolarization events in both Ctrl and mSod1 embryos. Moreover, the treatment with riluzole brings mSod1 motor neurons and interneurons spontaneous depolarization frequency to a value similar to that of Ctrl animals before riluzole treatment. These results strongly suggest a direct involvement of the persistent sodium current I_{NaP} in the mSod1 embryos neuronal hyperexcitability.

The increased activity of the persistent (non-inactivating) sodium current I_{NaP} in ALS has already been hypothesized in several studies performed in mice (Kuo et al., 2005; Van Zundert et al., 2008; Pieri et al., 2009). In acute brain slice and cultured neurons prepared from human SOD1 G93A mice, I_{NaP} amplitude measured at the peak of Current/Voltage relationship and current density is significantly higher compared to control neurons (Pieri et al., 2009). Interestingly, riluzole proved to be able to markedly block I_{NaP} and rapidly decrease firing frequency both in wild-type and mutant SOD1 expressing neurons (Kuo et al., 2005; Pieri et al., 2009). Although I_{NaP} represents a small fraction of the total neuronal

current (0.8-1%), it can deeply affect neurons and network behavior. This current, in fact, enhances neuronal excitability near firing threshold and is essential for spikes generation during sustained inputs (Urbani & Belluzzi, 2000). Since I_{NaP} can be activated at values close to the cell's resting potential, small increases in this current can enhance cell intrinsic excitability, alter spike initiation, and amplify the firing rate. In addition, the excitatory synaptic inputs received by a given neuron can be greatly amplified and prolonged by I_{NaP} thereby impacting the neuron's output by increasing its firing rates in response to synaptic modulation (Urbani & Belluzzi, 2000; Van Zundert et al., 2012).

The role played by I_{NaP} is extremely important for the modulation of the developing locomotor network in zebrafish embryo in normal condition. In fact, in coiling stage, 20-25 hpf, IC interneurons baseline membrane potential (membrane potential during inactive periods) does not differ significantly from I_{NaP} threshold, suggesting that this current is engaged at rest and IC cells possess I_{NaP}-dependent pacemaker properties (Tong et al., 2012). As IC interneurons directly contact several motor neurons along the same hemi-segment, synchronizing their firing, this could explain why this increased I_{NaP} activity and IC firing rate results in an increase in the relative percentage of tail coilings on the same side of the body. The direct and precocious involvement of interneurons in this disease model has been also addressed by McGown and colleagues who first observed heat shock stress response (HSR) in inhibitory glycinergic interneurons at 24 hpf and revealed that HSR was followed by a reduction in glycine release at 96 hpf (McGown et al., 2012).

The direct correlation between neuronal hyperexcitability and abnormal motor behavior was demonstrated by the fact that riluzole treatment significantly reduced the frequency of spontaneous tail coilings, the percentage of multiple coilings and the percentage of embryos performing multiple and complex coilings in mSod1 embryos. Furthermore, similarly to the effect on the frequency of spontaneous depolarization; the frequency of spontaneous coiling, the percentage of multiple tail coilings and the relative percentage of alternating and same-side tail bends in mSod1 embryos were brought to levels comparable to those of Ctrl embryos before riluzole administration.

Although we did not test the effect of riluzole on touch evoked tail coilings and touch evoked swimming, we might hypothesized that the overall increase in the motility of mutant embryos and larvae could be also associated to the persisting increase in the locomotor network excitability at 48 and 96 hpf. In this latter case, the increase in the motor neurons firing rate resulting from this condition, could prevail on the deficit in the neurotransmission that might be associated to the lower development of mature

neuromuscular junctions. The polyinnervation of zebrafish muscle fibers may contribute to the capability to perform the swimming behavior also in a partially denervated condition, but the reduction in the cholinergic stimulation might explain the reduction in muscle fibers caliber. We could also hypothesize that the loss of inhibitory inputs, due to the reduction in glycine release at 96 hpf, measured in *in vivo* patch clamp recordings in Sod1 G93R zebrafish (McGown et al., 2012), could be responsible for the increased motility at this developmental stage.

In our experimental condition, riluzole treatment significantly increased motor axons length in mSod1 embryos. This effect was unexpected because of the very short period of riluzole incubation (15-20 minutes) and the time of action before fixation (few hours), but it will be interesting to evaluate the effect of a prolonged riluzole administration to motor nerve morphology. Anyway, at the moment, we cannot say that the peculiar motor axons morphology of mutant embryos is a direct consequence of the alteration of mSod1 motor neurons excitability even if several papers demonstrated that altered neuronal electrical properties are associated with morphological defects (Van Zundert et al., 2008; Amendola & Durand, 2008; Martin et al., 2013).

Unfortunately, both the protein-channel and the gene responsible for I_{NaP} current are unknown at the moment; therefore it is still not known the relationship between Sod1 protein and I_{NaP} or the mechanism through which Sod1 mutation modify I_{NaP} activity. We should also stress that evidence of neuronal hyperexcitability are not a peculiar feature of ALS pathology associated to SOD1 mutations: motor neurons, differentiated from iPSC generated from cells obtained in human ALS patients harboring SOD1, C9orf72 and FUS mutations showed signs of hyperexcitability (Wainger et al., 2014), the studies conducted in the wobbler mouse, an ALS model carrying a point mutation in the Vps54 gene exhibit signs of cortical and hippocampal excitability already in the presymptomatic phase of the disease with a concomitant reduction in inhibitory paravalbumin positive interneurons in the symptomatic stage of the disease (Thielsen et al., 2013) and whole-cell recordings of CaP motor neurons in zebrafish embryos transiently expressing mutant FUS at 48 hpf displayed reduced rheobase current and higher frequencies of actions potentials following current injection when compared with control animals (Armstrong & Drapeau, 2013).

Results obtained in this research are still far from a clear identification of the mechanisms at the basis of such a complex pathology as ALS is and it will be necessary to accomplish further experiments to complete this picture. However, the data collected in

this work seem to fit with a very recent model generated in the attempt to explain neuronal vulnerability in ALS. This model postulates that the major costs on the energetic balance of neurons, and in particular of motor neurons, are synaptic activity and excitability: action potentials might consume more than a third of the overall ATP pool in a neuron. In a healthy neuron, the amount of ATP required for ion homeostasis under spontaneous or synaptically driven firing conditions is closely matched by the amount of ATP generated by the metabolic cascade. When higher-frequency firing is imposed, the amount of ATP generated cannot sustain the activity of Na^+/K^+- ATPase and the ion balance starts drifting away from the homeostatic set point. With increasing firing rates and decreasing ATP production, the motor neuron is driven into an unstable condition, where the higher the load of ionic imbalances, the less ATP is available for compensation. In addition, the energetic imbalance is further worsened by the rising Ca^{2+} concentration due to mitochondrial overload, leading to further reduced ATP synthesis, so that even small initial energy deficits are amplified by increasing mitochondrial failure. Finally, the motor neuron crashes into a state of depolarization, when it can no longer fire, although the energetic load keeps increasing. According to this model small original imbalances can lead to motor neurons failure if enough time and sufficient high-frequency firing are allowed, suggesting that energetic mismatch could pile up during the lifetime of a motor neuron at different rates due to different firing properties and patterns (Roselli & Caroni, 2014).

We could therefore hypothesize that this small precocious increase in the I_{NaP} mediated depolarization frequency of the zebrafish locomotor network could lead to the progressive motor neurons dysfunctions such as impairment in axonal transport and mitochondria alterations, leading to degeneration and ultimately to ALS development.

Our study addresses another important issue in the study of ALS that is the identification of the way by which riluzole exerts its therapeutic action in slowing the progression of this disease. Riluzole effects are complex and still not completely understood; they involve the inhibition of the voltage-dependent sodium channels and also a reduction of glutamate release. The correlation of the two mechanisms, however, remains to be elucidated because tetrodotoxin, a sodium channel blocker, fails to mediate the same effect on glutamate release (Urbani & Belluzzi, 2000). At the recommended daily dose, the maximum plasma levels of riluzole range between 1–2 μM (with three to fourfold higher concentrations in brain tissue), these therapeutic concentrations of riluzole might be well in the range where an appreciable reduction of I_{NaP} would be expected; in contrast,

inhibition of the fast Na^+ current is achieved by riluzole only at doses that in mammals are well above therapeutic doses (Urbani & Belluzzi, 2000; Bellingham, 2011).

Beyond the mechanism of action, another concern related to riluzole is linked to the timing of riluzole treatment. In transgenic SOD1 G93A ALS mice starting the drug administration at P30–P50 delays death by only 9–14 days. This modest delay in survival after riluzole treatment is disappointing from a therapeutic and conceptual point of view, especially when considering that riluzole did not significantly affect disease onset (Bellingham, 2011). These studies need, however, to be considered in view that electrophysiological abnormalities that are likely targeted by riluzole are initiated much earlier (P4–P10) (Van Zundert et al., 2008) than the start of the drug treatment in these studies (P30–P50) (Bellingham, 2011).

Our work, together with several other recent evidence, points out that increased excitability and neuronal activity during very precious developmental stages might induce a pathophysiological cascade of events that cannot be reversed by later riluzole treatment.

CONCLUSION

This work demonstrates that the Sod1 G93R zebrafish model represent a valuable complement to other animal model for the study of Amyotrophic Lateral Sclerosis.

Adult zebrafish expressing mutant Sod1 develop most of the main pathological features occurring in ALS that have already been well identified and documented in humans and other animal models of the disease: locomotor impairments, motor neurons degeneration and spinal cord atrophy, neuromuscular junctions loss, muscle fibers atrophy, ultrastructural alterations at the nerves terminals and muscles, astrogliosis and inflammation.

This model proves to be a powerful model on its own in the study of ALS mainly thanks to the advantages associated to the possibility to study locomotor circuits at the very early stages of development and for the accessibility of this model for genetic manipulation and microscopic investigation.

Mutant zebrafish embryos and larvae display precocious morphological alterations affecting the locomotor network: defective motor nerves outgrowth and neuromuscular junctions maturation impairment. Moreover, they present concomitant motor impairments. This model offers the unique situation for the study of a simple spinal cord functional circuit, capable to give rise to a motor response dependent exclusively on electrical coupling. Thanks to this advantage, we identified in Sod1 G93R expressing embryos spinal neurons hyperexcitability associated to the increased activity of the persistent sodium current I_{NaP} before the superimposition of the chemical transmission.

By administering riluzole directly into the embryo water we demonstrated the possibility to pharmacologically modify behavioral phenotype, spinal neurons electrical activity and motor axons length.